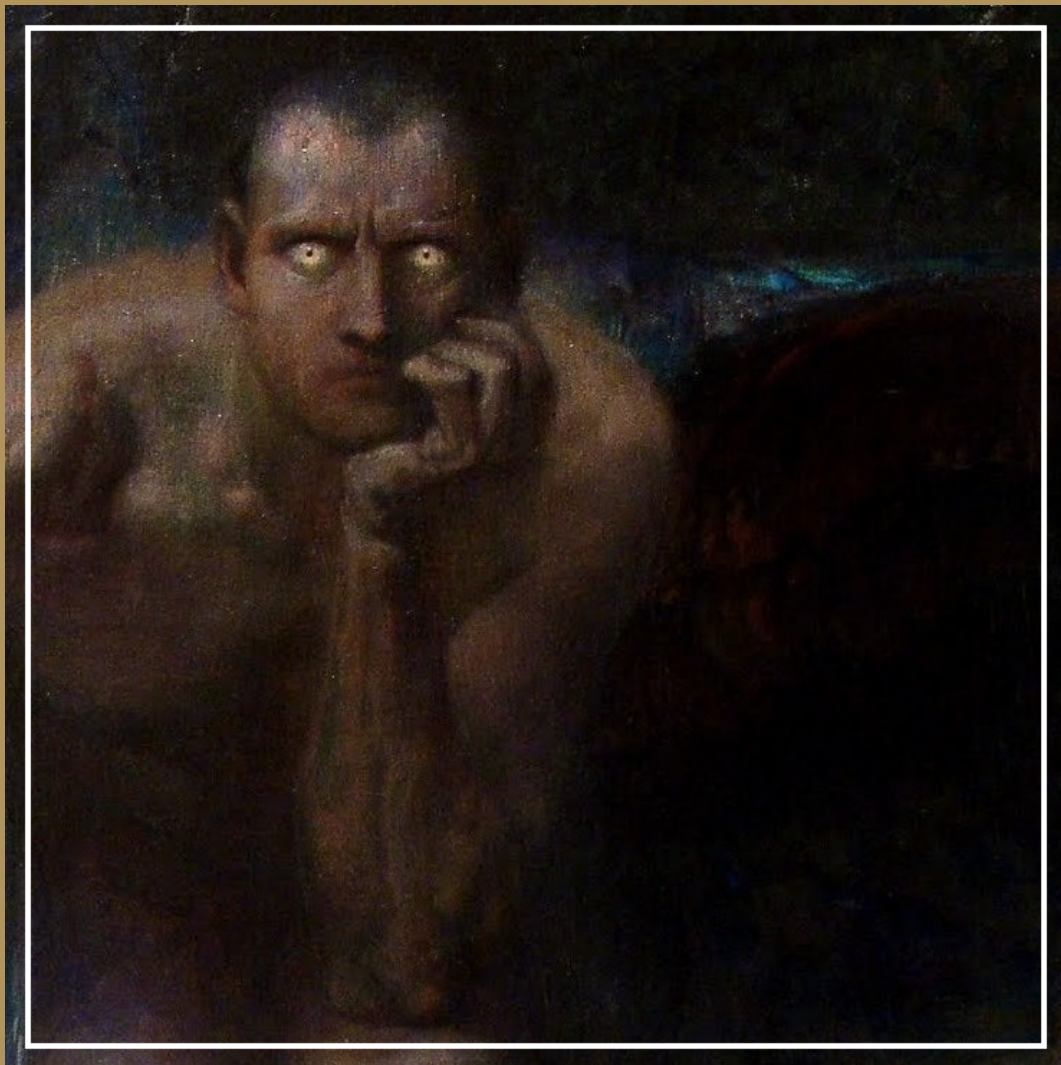


Journal notes on:

# Topological superconductivity

by Francisco Lobo





## CONTENTS

Acknowledgments	5
Preface	6
Ongoing research endeavors	7
<b>I Introduction to topological superconductivity</b>	8
I. Concepts of symmetry and topology	8
A. Introduction to topological invariants in 0D models	10
1. Time-reversal symmetry	10
2. Sublattice symmetry	11
3. Particle-hole symmetry	12
4. Combining symmetries	13
B. Introduction to topological invariant in higher dimensions.	13
1. Berry connection and Chern number.	13
2. Aharonov-Bohm effect	15
3. Quantum Thouless pump	16
II. Topological superconductivity in 1D models	16
A. Kitaev model	16
1. Majorana modes at a domain wall	20
2. Kitaev ring	21
3. Doublet Kitaev chain	21
B. SSH model	21
C. Oreg-Lutchyn models	21
III. Topological superconductivity in 2D models	24
A. Integer quantum hall effect	24
1. Classical Hall effect and Landau quantization	24
2. Quantum Hall chiral edge states	26
3. Non-interacting electrons in a Corbino disk	28
B. Anomalous quantum Hall effect	29
1. Graphene's discrete symmetries	30
2. Haldane's graphene model and chirality	30
3. Gap closings are sources of Berry curvature	31
4. Chiral edge states in graphene zigzag ribbons	32
C. Quantum spin Hall effect	34
1. Kane-Mele graphene model	34
D. Fractional quantum hall effect	34
<b>II Appendix</b>	35
IV. Overview of graphene systems	35
A. Standard monolayer graphene	35
B. Kekulé modulation	38
C. Bilayer graphene	38
1. Bernal bilayer graphene	38

2. Armchair and Zigzag configurations	40
D. Twisted bilayer graphene	40
E. Trilayer graphene	40
<b>III Bibliography</b>	<b>41</b>
References	41

## ACKNOWLEDGMENTS

Given their nature as personal journal notes, these sections remain perpetually incomplete and are subject to ongoing revision. While you are more than welcome to read them, please be advised that they may contain errors or misinterpretations on my part. If your expertise or intuition suggests that something appears inaccurate or questionable, your assessment is likely correct. Should you identify any such issues, I would be deeply grateful if you could contact me regarding the matter, as this would allow me to make corrections and further my understanding.

Alongside these personal journal notes, an accompanying worksheet is provided. Given that the notes primarily emphasize physical intuition and conceptual depth rather than rigorous mathematical derivations, lengthier or more tedious calculations have been separated into this supplementary material to maintain clarity and focus in the main text. These exercises are referenced at relevant points, particularly following claims that may appear mathematically abrupt. If a result seems unclear at first glance, the reader may consult the exercise sheet for a complete derivation. These exercises largely constitute "do once in a lifetime" endeavors, as their derivations hold no hidden complexity upon inspection. Having demystified them, one may thereafter accept the results without repeating the process. As another supplementary material, there is a GitHub repository at <https://github.com/francisco1880/topoSC> where you can check the code that generate the figures of the various models. This is done in *Julia* using the *Quantica.jl* package by Pablo San-Jose, my PhD advisor. Check *Quantica.jl*'s repository and it's tutorial at <https://github.com/pablosanjose/Quantica.jl>. Additional journal entries on related topics can be found on my personal website at <https://francisco1880.github.io/>. These may serve as supplementary material to the present notes. In particular, I recommend the one titled "Introduction to Many-Body Theory in Condensed Matter Physics", which provides a foundational overview of key concepts in condensed matter physics and serves as a useful precursor to the material discussed here.

I would like to express my sincere gratitude to my advisors, Pablo San-Jose and Elsa Prada, for their invaluable guidance, support, and mentorship throughout the course of my thesis. Their broad expertise has been instrumental in the development of this book, especially considering that many of its core topics first emerged as recurring themes I encountered during our thesis meetings. In particular, Elsa Prada's presentation on Topological Insulators and Superconductors served as a key inspiration and provided the initial conceptual framework from which this book began to take shape.

I am also deeply grateful to my colleagues, César Robles and Carlos Paya, as well as to my good friend, Tiago Antão, for their assistance and for the many stimulating and insightful discussions we shared. Their input has significantly contributed to the refinement of my ideas and the overall coherence of this work.

## PREFACE

This book originates from the foundational work undertaken during my Master's thesis, entitled "**TITLE**", wherein the initial years of study were primarily devoted to the core topics presented herein. As such, the structure and substance of this text mirror the intellectual journey of a graduate student encountering the field of superconductivity for the first time. This was written from a PhD student point-of-view with the intention of guiding fellow PhD students (or any early-career researchers) through the essential theoretical frameworks that form the backbone of both conventional and emerging theories of superconductivity. The material is deliberately presented in an expository and intuitive manner, prioritizing physical insight and conceptual clarity over rigorous mathematical derivation. This stylistic choice reflects the pedagogical aim of the book. I wish not to exhaustively cover each subject, but to serve as an accessible entry point into concepts that are often referenced but rarely unpacked in detail within advanced literature. Accordingly, this work is best viewed as a primer, one that provides a conceptual map and intuitive scaffolding for readers new to the field, while simultaneously functioning as a compact memory aid for those revisiting these topics. Researchers requiring deeper or more specialized knowledge are encouraged to consult the original papers, which are duly noted at the beginning of each section (**note yet though**), that rigorously address each subject in its full technical detail.

The rest of the preface will be written when the book is mostly finished.

## ONGOING RESEARCH ENDEAVORS

I intend to compose various paragraph detailing the research endeavors of my fellow colleagues pursuing studies in the field of topological superconductivity. This exposition will serve as a representative landscape of current investigative directions within the field, as reflected through the diverse yet interrelated topics being explored by peers in the discipline.

## Part I

# Introduction to topological superconductivity

## I. CONCEPTS OF SYMMETRY AND TOPOLOGY

Topology studies whether objects can be transformed continuously into each other. In condensed matter physics we can ask whether the Hamiltonians of two different systems can be continuously transformed into each other. If that is the case, then we can say that two systems are ‘topologically equivalent’.

In order to understand the concept of topology in condensed matter in the simplest way possible let us consider the transformation of a system described by the Hamiltonian  $\mathcal{H}$  by the tuning of some external parameter  $\alpha$  such that at  $\mathcal{H}_i \equiv \mathcal{H}(\alpha = 0)$  is the initial state Hamiltonian and  $\mathcal{H}_f \equiv \mathcal{H}(\alpha = 1)$  the final. Understand that the transformation of  $\mathcal{H}$  must be physical, meaning that it should be just a matter of point of view. Because of this, not only must  $\mathcal{H}$  be an hermitian matrix, i.e  $\mathcal{H} = \mathcal{H}^\dagger$  (such that it has real eigenenergies), but also that any transformation must be isometric (aka norm-preserving) isomorphisms (aka one-to-one mapping). Due to Wigner’s theorem these transformations can either be unitary  $\mathcal{U}$  or anti-unitary  $\bar{\mathcal{U}}$ . A unitary transformation between two inner product spaces reads as  $\langle \mathcal{U}\varphi | \mathcal{U}\psi \rangle = \langle \varphi | \psi \rangle$  while an anti-unitary transformation reads instead as  $\langle \bar{\mathcal{U}}\varphi | \bar{\mathcal{U}}\psi \rangle = \langle \varphi | \psi \rangle^* = \langle \psi | \varphi \rangle$ . Of course, any anti-unitary operator can be written as the product of a unitary operator and the complex conjugation operator  $\mathcal{K}$ .

### *Unitary transformations*

Unitary transformations do not have particularly interesting consequences for topological classification. Consider an Hamiltonian  $\mathcal{H}$  with the symmetry constraint  $\mathcal{U}^\dagger \mathcal{H} \mathcal{U} = \mathcal{H}$ . See that  $\mathcal{H}$  commutes with  $\mathcal{U}$  meaning that the system has a conservation law, and that the Hamiltonian can be brought to a block-diagonal form

$$\mathcal{H} = \left( \begin{array}{c|c} \mathcal{H}^{(1)} & \\ \hline & \mathcal{H}^{(2)} \end{array} \right), \text{with } \mathcal{H}^{(n)} = \left( \begin{array}{c|c} h_{11} & h_{12} \\ \hline h_{12}^* & h_{22} \end{array} \right). \quad [1]$$

This procedure can be repeated until one runs out of unitary symmetries and is left with an irreducible block of the Hamiltonian, i.e. one which cannot be block diagonalized. In this case, every one of those  $\mathcal{H}_i^{(n)}$  Hamiltonians at the  $n$  block-diagonal could be continuously deformed into  $\mathcal{H}_f^{(n)}$ , meaning that they are always topologically equivalent.

### *Introduction to CPT symmetries*

One the other hand, anti-unitary transformations do impose constraints on an irreducible Hamiltonian, for example, by forcing it to maintain a (physically) finite energy gap, or to be a real matrix, or to be block off-diagonal. In this case, telling if  $\mathcal{H}_i$  and  $\mathcal{H}_f$  are topologically equivalent is not trivial. There are three fundamental discrete symmetries: chiral symmetry (CS)  $\mathcal{C}$ , parity symmetry  $\mathcal{P}$ , time-reversal symmetry (TRS)  $\mathcal{T}$ , known collectively as CPT symmetry. In a condensed matter picture, we often refer to the chiral symmetry as being a sublattice lattice and the parity symmetry as a particle-hole symmetry (PHS). Sublattice symmetry means that our system can be naturally split into two interpenetrating sublattices. The Hamiltonian connects only sites from these different sublattices and, as a result, it anticommutes with an operator that distinguishes between them. Particle-hole symmetry means that for every electronic state with energy  $\varepsilon$  there is a corresponding electron-hole (as in absence of an electron) state, at  $-\varepsilon$ . Hence, mirroring the electron’s occupancy along the Fermi level, meaning that occupied becomes unoccupied and vice versa, the spectrum remains unchanged. Finally, time reversal symmetry means that our system would have behave the same if time flown backwards. In this backward time frame momentums change sign and spins flip.

There is, however, an important detail: both  $\mathcal{T}$  and  $\mathcal{P}$  are indeed anti-unitary transformations but  $\mathcal{C}$  is not. This is because whenever a system has both TRS and PHS there is also a chiral symmetry

$\mathcal{C} = \mathcal{PT}$ . This also means that if a system only has either but not both, it cannot have a chiral symmetry. In other words, the presence of any two out of the three symmetries implies that the third is also present. Since the product of two anti-unitary operators is a unitary operator then  $\mathcal{C}$  must be unitary. Also, see that if both TRS and PHS are absent, then CS may or may not be present. In these two situations, formally known as *classes*, there are no anti-unitary symmetries, furthering their classification to *complex classes*.

Another important detail is that for TRS we have that  $[\mathcal{H}, \mathcal{T}] = 0$  while for PHS we have that  $\{\mathcal{H}, \mathcal{P}\} = 0$ . By implication of what we just talked, also  $\{\mathcal{H}, \mathcal{C}\} = 0$ .

Furthermore, as the next and final note about this symmetries, know that TRS and PHS may come in two separate flavors, depending on whether they square to plus or minus one. So, for example, a system can behave in three ways concerning TRS: (1) it does not have TRS, (2) it has it and  $\mathcal{T}^2 = +1$  (3) it has it and  $\mathcal{T}^2 = -1$ . On the other hand, the chiral symmetry only comes in one flavor,  $\mathcal{C}^2 = +1$ . Due to flavor combinations we find a total of 10 distinct symmetry classes displayed in figure [1]. The classifications  $\mathbb{Z}$ ,  $2\mathbb{Z}$  and  $\mathbb{Z}_2$  on the left are to be introduced in the following examples.

class	$\mathcal{C}$	$\mathcal{P}$	$\mathcal{T}$	$d = 0$	1	2	3
A				$\mathbb{Z}$		$\mathbb{Z}$	
AI			1	$\mathbb{Z}$			
AII			-1	$2\mathbb{Z}$		$\mathbb{Z}_2$	$\mathbb{Z}_2$
AIII	1				$\mathbb{Z}$		$\mathbb{Z}$
BDI	1	1	1	$\mathbb{Z}_2$	$\mathbb{Z}$		
C		-1				$2\mathbb{Z}$	
CI	1	-1	1			$2\mathbb{Z}$	
CII	1	-1	-1		$2\mathbb{Z}$		$\mathbb{Z}_2$
D		1		$\mathbb{Z}_2$	$\mathbb{Z}_2$	$\mathbb{Z}$	
DIII	1	1	-1	$\mathbb{Z}_2$	$\mathbb{Z}_2$	$\mathbb{Z}_2$	$\mathbb{Z}$

Figure 1. Symmetry periodic table with Altland-Zirnbauer classification. For more details on this table, for example, on how to go from  $d = 0$  to  $d > 0$  by adding and removing symmetries and it's Boot clock patterns see Akhmerov's "10 symmetry classes and the periodic table of topological insulators" at [https://topocondmat.org/w8\\_general/classification.html](https://topocondmat.org/w8_general/classification.html).

It is important to have in mind that CPT symmetries may not be the only symmetries at play. Although these are the fundamental symmetries, if one works within a condensed matter framework, the underlying lattice will provide additional, often spatial, symmetries. These include, for example point group symmetries—involution, mirror, and rotational symmetries—and space group symmetries—translation, glide, or screw symmetries of the entire crystal lattice. Point group symmetries protect additional degeneracies or enforce selection rules that are not captured by the non-spatial discrete symmetries alone, for example, a mirror symmetry in a crystal that protects gapless modes on certain surfaces or edges that are invariant under reflection. One the other hand space group symmetries constrain the electronic band structure and can lead to phenomena like Dirac or Weyl points that interact with the superconducting pairing.

### A. Introduction to topological invariants in 0D models

In order to study the effects of these symmetries, let us imagine a panoply of different systems and their energy spectrums as a function of  $\alpha$ . Moreover, let us count the number of levels below zero energy (defined at the Fermi level  $\varepsilon_F$ ) at each different  $\alpha$ , denoting it with  $Q$ . This will be our topological invariant prototype. If  $Q$  is the same in the initial and final system and did not change along the tuning of  $\alpha$  then there must be a continuous transformation Hamiltonian which does not close the gap. One the other hand, if  $Q$  changes then the system are *not* topologically equivalent as it would be needed to close the (physically real) gap. Hence, such a crossing changes the topological invariant, dubbed topological phase transition.

For all the examples that follow we assume a zero-dimensional ( $d = 0$ ) system. In a condensed matter realization this could be, for instance, a quantum dot interaction with all kinds of external systems. This will become

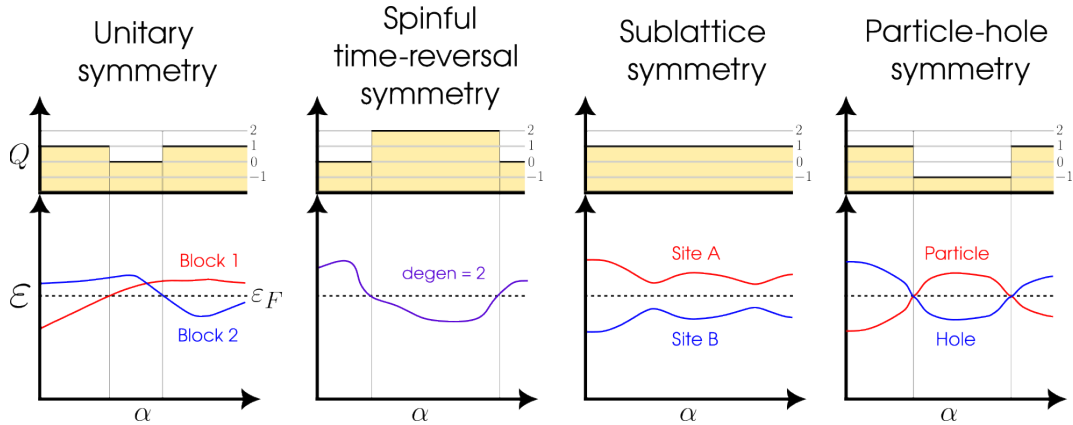


Figure 2. Kitaev chain Majorana modes pairing possibilities tbh I still don't fully understand why I can't just change the Fermi energy? I mean, for the spinful TRS I could only get 0 or 2 still. Does the spectrum of the CS and PHS just translate along with  $\varepsilon_F$  while the unitary does not?

#### 1. Time-reversal symmetry

Time-reversal symmetry is represented by an anti-unitary operator, and as such it can always be written as the product  $\mathcal{T} = U\mathcal{K}$  with  $U$  an unitary matrix and  $\mathcal{K}$  complex conjugation. A real Hamiltonian is a manifestation of time-reversal symmetry.

##### Spinless case

For example, for a spinless system we have  $\mathcal{T} = \mathcal{K}$  and thus  $\mathcal{T}\mathcal{H}\mathcal{T}^{-1} = \mathcal{H}^* = \mathcal{H}$  is a real matrix. In this case the TRS flavor is positive i.e  $\mathcal{T}^2 = +1$ . Still, this case is also not interesting because is not different from the previous one, the different energy levels move and the topological invariant changes by one when one of them crosses zero. In this trivial case the topological invariant is an integer number,  $Q = 0, \pm 1, \pm 2, \dots \in \mathbb{Z}$ . I mean, it should be  $\mathbb{N}$  no? How would the negative numbers appear?

##### Spinful case

There is, however, a very important case where time-reversal symmetry makes a real difference. For a 1/2-spin system we the time-reversal operator reads

$$\mathcal{T} = i\sigma_y\mathcal{K} \quad [2]$$

with  $\sigma_y = [ 0 \ -i ; +i \ 0 ]$  the 2nd Pauli matrix (we reserve  $\sigma$  for Pauli matrices in spin orbital space). In this case the flavor is negative, i.e  $\mathcal{T}^2 = -\mathbf{1}$ , and

$$\mathcal{T}\mathcal{H}\mathcal{T}^{-1} = \sigma_y \mathcal{H}^* \sigma_y = \mathcal{H} \quad [3]$$

meaning that every energy eigenvalue  $\varepsilon$  is doubly degenerate. This happens because both the electrons with spin up or down have the same eigenenergy. This doubly degeneracy is often refer to as Kramers' degeneracy. Such a Hamiltonian would read in matrix form as

$$\mathcal{H} = \left( \begin{array}{c|c} \varepsilon_1 \mathbf{1} & M \\ \hline M^\dagger & \varepsilon_2 \mathbf{1} \end{array} \right) = \left( \begin{array}{cc|cc} \varepsilon_1 & 0 & m_{11} & m_{12} \\ 0 & \varepsilon_1 & -m_{12}^* & m_{11}^* \\ \hline m_{11}^* & -m_{12} & \varepsilon_2 & 0 \\ m_{12}^* & m_{11} & 0 & \varepsilon_2 \end{array} \right). \quad [4]$$

with  $\varepsilon_1, \varepsilon_2$  real numbers.

We can see the consequences of Kramers' degeneracy on the band spectrum versus  $\alpha$  in figure [2]. While the spectrum looks quite similar to the previous ones, whenever a line crosses zero energy, our topological invariant makes a jump of two, and not one! In this case, time-reversal symmetry constrains the topological invariant to only take even values,

$$Q = 0, \pm 1, \pm 2, \dots \in 2\mathbb{Z}. \quad [5]$$

This is an example of how topological properties can be influenced by discrete symmetries.[1]

## 2. Sublattice symmetry

We just saw that time-reversal symmetry can forbid the topological invariant to take a certain set of values. We now study another case where a symmetry changes the topological properties dramatically.

Let's now take a system where we can split all the degrees of freedom into two groups—group  $A$  and group  $B$ —, such that the Hamiltonian only has nonzero matrix elements between two groups, and not inside each group. This situation arises naturally when the a given lattice has two sublattices. For example, for hexagonal boron nitrate (hBN) we can distinguish these sublattices as the boron and nitrogen sites respectively. The matrix of such an Hamiltonian would read

$$\mathcal{H} = \left( \begin{array}{c|c} M & \\ \hline M^\dagger & \end{array} \right) = \left( \begin{array}{cc|cc} 0 & 0 & m_{11} & m_{12} \\ 0 & 0 & m_{21} & m_{22} \\ \hline m_{11}^* & m_{21}^* & 0 & 0 \\ m_{12}^* & m_{22}^* & 0 & 0 \end{array} \right). \quad [6]$$

See that  $\eta_z \mathcal{H} \eta_z = -\mathcal{H}$  where  $\eta_z = [ +1 \ 0 ; 0 \ -1 ]$  is the 3rd Pauli matrix (we reserve  $\eta$  for Pauli matrices in sublattice orbital space). This immediately means that if  $\Psi = [ \psi_A; \psi_B ]^T$  is an eigenvector of the Hamiltonian with energy  $\varepsilon$ , then  $[ \psi_A; -\psi_B ]^T$  is an eigenvector with energy  $-\varepsilon$ . A symmetric spectrum is the consequence of sublattice symmetry as seen in figure [2]. This means that  $Q$  always stays constant and that we can always deform Hamiltonians with sublattice symmetry without closing the gap. This indicates that an extra symmetry, such as this one, may render the topology of a system as trivial.

### 3. Particle-hole symmetry

Another symmetry that has a strong influence on topology is the particle-hole symmetry, showing up in superconducting systems. As we saw in BCS theory, a superconductor will create(annihilate) pairs of electrons by breaking(forming) Cooper pairs costing a pairing energy of  $\Delta$  to the system.

Let us consider that the dynamics of the electrons is described by the an hermitian  $H$  matrix while the pair creation and annihilation is described by an antisymmetric  $\Delta$  matrix. Understand that  $\Delta$  must antisymmetric just because because the fermion operators anticommute. The Hamiltonian describing the full system reads

$$\mathcal{H} = \left( \begin{array}{c|c} H & \Delta \\ \hline -\Delta^* & -H^* \end{array} \right) = \left( \begin{array}{cc|cc} h_{11} & h_{12} & 0 & \Delta \\ h_{12}^* & h_{22} & -\Delta & 0 \\ \hline 0 & -\Delta^* & -h_{11}^* & -h_{12}^* \\ \Delta^* & 0 & -h_{12} & -h_{22}^* \end{array} \right) \quad [7]$$

and is know as the Bogoliubov-de Gennes (BdG) Hamiltonian. Moreover, we now double the amount of degrees of freedom in the system by defining a Nambu spinors

$$\check{c}_i^\dagger = \begin{pmatrix} c_i^\dagger & c_i \end{pmatrix} \quad \text{and} \quad \check{c}_i = \begin{pmatrix} c_i \\ c_i^\dagger \end{pmatrix} \quad [8]$$

such that we can write

$$\check{\mathcal{H}} = \frac{1}{2} \check{c}^\dagger \mathcal{H} \check{c}.$$

This definitions indicates that the Bogoliubov-de Gennes Hamiltonian acts not only on electrons but also on an extra mirror set comprised of eletron-holes. Since holes are related to the electrons,  $\mathcal{H}$  automatically inherits that extra symmetry. This symmetry exchanges electrons with holes, and has an anti-unitary operator  $\mathcal{P} = \tau_x \mathcal{K}$  with  $\tau_x = [0 \ 1; 1 \ 0]$  the 1st Pauli matrix (we reserve  $\sigma$  for Pauli matrices in spin orbital space) and (as before)  $\mathcal{K}$  complex conjugation. Hence we have that  $\mathcal{P}\mathcal{H}\mathcal{P}^{-1} = -\mathcal{H}$ . For this specific case it's flavor is positive, i.e  $\mathcal{P}^2 = +1$ . Indeed, for every eigenvector  $\Psi = [u; v]^T$  with energy  $\varepsilon$ , there will be a particle-hole symmetric eigenvector  $\mathcal{P}\Psi = [v^*; u^*]^T$  with energy  $-\varepsilon$ . As clearly seen in figure [2], because of the minus sign in the particle-hole symmetry, the spectrum of  $\mathcal{H}$  must be mirrored around zero energy, that is, the Fermi level).

#### Fermionic parity switches

See that this spectrum mirroring was also the case for sublattice symmetry however, in this case, energy levels do not repel around zero energy, so that crossings at zero energy appear. Unlike in the case of sublattice symmetry, a pair of  $\pm\varepsilon$  energy levels does not corresponds to two distinct quantum states, but to a single quantum state. This quantum state is a coherent superposition of electrons and holes, a so called Bogoliubov quasiparticle. It has an excitation energy  $\varepsilon$ , and it is created by an operator  $\gamma^\dagger = uc^\dagger + vc$ . Populating the partner state at energy  $\varepsilon$  is the same as emptying the positive energy state.

In general a crossing between energy levels happens in the presence of a conserved quantity. While the mean-field Hamiltonian of a superconductor does not conserve the number of particles, it conserves the parity of this number. In other words, forming and breaking Cooper pairs does not affect whether the superconducting contains an even or odd number of electrons so fermion parity is a conserved quantity (provided that isolated electrons do not enter or leave the system). Fermion parity, however, is a many-body quantity, which cannot be directly described in terms of the single particle picture of the BdG Hamiltonian. This is why we had to double the number of degrees of freedom by hand. When a pair of levels crosses zero energy, the excitation energy  $\varepsilon$  of the Bogoliubov quasiparticle changes sign and it becomes favorable to add(remove) a Bogoliubov quasiparticle. In other words, at each crossing the fermion parity in the ground state changes from even to odd (or vice versa), meaning that these crossings are fermion parity switches.

### *The Pfaffian invariant*

Since the ground state fermion parity is preserved by the superconducting Hamiltonian if there are no Bogoliubov quasiparticles crossing zero energy, the ground state fermion parity is the topological invariant of this system. It is clear however that this invariant is of a different nature than the one of the non-superconducting systems, which is given by the number  $Q$  of negative eigenvalues of the Hamiltonian. The latter cannot change for a BdG Hamiltonian, which has a symmetric energy spectrum, and hence it is not suitable to describe changes in fermion parity. For this kind of systems the actual topological invariant is called the *Pfaffian* and will either take the value  $Q = \pm 1 \in \mathbb{Z}_2$  at every zero-energy crossing. Its rigorous definition is not really that important for our sake so we take a simpler approach.

In order to introduce the Pfaffian invariant, we start by making a basis transformation  $\mathcal{H}'_{\text{BdG}} = \mathcal{U}\mathcal{H}_{\text{BdG}}\mathcal{U}^\dagger$  that makes the Hamiltonian an skew-symmetric matrix, i.e  $\mathcal{H}^T = -\mathcal{H}$ . We do this because the eigenvalues of antisymmetric matrices always come in pairs, i.e  $\pm \varepsilon_n$ . Further reasoning will become apparent as we go. Such a transformation is

$$H'_{\text{BdG}} = \frac{1}{2} \begin{pmatrix} 1 & 1 \\ i & -i \end{pmatrix} H_{\text{BdG}} \begin{pmatrix} 1 & 1 \\ i & -i \end{pmatrix} = \frac{1}{2} \begin{pmatrix} H - H^* + \Delta - \Delta^* & i(-H - H^* + \Delta + \Delta^*) \\ i(+H + H^* + \Delta + \Delta^*) & H - H^* - \Delta + \Delta^* \end{pmatrix}$$

Indeed, because  $H$  is Hermitian then  $H - H^*$  is antisymmetric and  $H + H^*$  is symmetric, i.e  $\mathcal{H}^T = \mathcal{H}$ ; since  $\Delta$  is antisymmetric then  $H'_{\text{BdG}}$  is also antisymmetric. In its diagonalized form the determinant of this matrix is just the product of the pairs of eigenenergies, i.e  $\det(\mathcal{H}) = \prod_n (-\varepsilon_n^2)$ . The key feature of the Pfaffian is revealed when taking now the square root of the determinant  $\text{Pf}(\mathcal{H}) = \sqrt{\det(\mathcal{H})} = \pm \prod_n i\varepsilon_n$ . See that it is defined in such a way that the sign of the product is uniquely defined. At a fermion parity switch a single  $\varepsilon_n$  changes sign, so the Pfaffian changes sign as well while the determinant stays the same. We then define the actual topological invariant as

$$Q_{\text{BdG}} = \text{sign} [\text{Pf}(i\mathcal{H})],$$

where we have included a factor of  $i$  just that the Pfaffian is a real number, such that at  $Q_{\text{BdG}}$  changes its value from  $+1$  to  $-1$  at every zero-energy crossing. This means that it is the correct expression for the ground state fermion parity and for the topological invariant. As some sort of intuition, you can think of it as if the number of holeonic levels below zero energy counts negatively to the overall positive electronic levels.

#### 4. Combining symmetries

##### *Particle-hole and spinful time-reversal symmetry*

Take a system that has both particle-hole symmetry (PHS) and spinful time-reversal symmetry (TRS) described by the Hamiltonian  $\mathcal{H}$ . Let us take an intuitive approach to the band spectrum analysis. By PHS we know that an electronic band is equivalent to a negative holeonic band. On the other hand, by spinful TRS we know that there is Kramer degeneracy. Hence, since a PHS holeonic band counts as negative to the number of bands below zero energy we will always end up with  $Q$  being even and changing sign at a crossing. *This is wrong but can't see the flaw in logic. I mean, looking at the table I can see that  $P^2 = 1$  and  $T^2 = -1$  gives me no constrain on  $Q$  and thus trivial topology.*

## B. Introduction to topological invariant in higher dimensions.

### 1. Berry connection and Chern number.

In higher dimensional system the discrete energy levels of a  $d = 0$  system are replaced by continuous energy bands defined along the Brillouin zone. In these higher dimensions the topological invariant

cannot be defined merely as counting levels below the Fermi energy or by tracking sign changes of the Pfaffian in superconducting systems. Instead, the central theme of  $d > 0$  dimensional band topology lies in the concept of geometric phases.

As an illustrative example of the concepts to come, consider a vector placed at the earth's north pole, always pointing in the tangent direction to the surface. If one translates the vector to the equator along a meridian, then along the equator for some distance, and back to the north pole, the vector's orientation will have changed relative to how it started by some angle. This angle is called the holonomy. The origin of non-trivial band topological properties is not so different from this example, with the crucial replacement of the vector by a Hamiltonian  $\mathcal{H}(\boldsymbol{\alpha})$  depending on a set of parameters  $\boldsymbol{\alpha} = (\alpha_1, \dots, \alpha_N)$ , and the earth a manifold (topological space that locally resembles Euclidean space near each point) spanned by those parameters. In the context of Hamiltonians, holonomy manifests as the acquisition of additional geometric phases by the eigenstate of  $\mathcal{H}(\boldsymbol{\alpha})$  as the parameter space manifold is traversed. More concretely, in band topology,  $\boldsymbol{\alpha}$  is taken to be the momenta  $\mathbf{k} = (k_1, \dots, k_d)$ , with  $d$  the space dimensions, together with a set of additional tunable parameters (chemical potential, electric field, Zeeman, integrated out pairing, etc, etc...), and the eigenstate's additional geometric phase is the so-called Berry phases (we will further explore this later concept in just a moment). In this context, the restriction that evolution is adiabatic simply means that the system must remain in a situation where energy bands do not cross, i.e. the system must be gapped.

The idea is that if the parameters  $\boldsymbol{\alpha}$  are varied adiabatically, then at each subsequent value of  $\boldsymbol{\alpha}$ , eigenstates of one set of parameters are smoothly deformed into another set. This is the content of the adiabatic theorem, which states that in the case of adiabatic evolution of the parameters along a curve  $\boldsymbol{\alpha}(t)$ , the Schrodinger equation

$$-i\hbar\partial_t |\psi_n(\boldsymbol{\alpha}(t))\rangle = \varepsilon_n(\boldsymbol{\alpha}(t)) |\psi_n(\boldsymbol{\alpha}(t))\rangle \quad [9]$$

is obeyed instantaneously. Here  $|\psi_n(\boldsymbol{\alpha}(t))\rangle$  represents the eigenstate of the Hamiltonian  $\mathcal{H}(\boldsymbol{\alpha}(t))$  in the  $n$ th band with energy  $\varepsilon_n(\boldsymbol{\alpha}(t))$ . Now, generically, due to the structure of the Schrodinger equation, and the normalization of states, a single degree of freedom exists, which can change the eigenstate as it is moved along the parameter space  $\boldsymbol{\alpha}(t)$ . This corresponds to a phase denoted by  $\theta(t)$ , such that the state can be decomposed as

$$|\psi(\boldsymbol{\alpha}(t))\rangle = e^{i\theta(t)/\hbar} |\phi(\boldsymbol{\alpha}(t))\rangle. \quad [10]$$

A short calculation performed by plugging this form of the state into the Schrodinger equation on both sides, and acting with  $\langle\psi(\boldsymbol{\alpha}(t))|$  on the left is enough to solve for the phase  $\theta(t)$ . One obtains

$$\theta(t) = \int_0^{t'} dt \left[ \varepsilon(\boldsymbol{\alpha}(t)) + \frac{i}{\hbar} \langle\phi(\boldsymbol{\alpha}(t))| \partial_t |\phi(\boldsymbol{\alpha}(t))\rangle \right] \quad [11]$$

There are two contributions to the phase acquired by the eigenstate under adiabatic evolution. The first term is the familiar dynamical phase  $\theta_D(t)$ , which is acquired from evolving in time in the Hilbert space. However, a second term appears, namely

$$\gamma(t) = \frac{i}{\hbar} \int_0^{t'} dt \langle\phi(\boldsymbol{\alpha}(t))| \partial_t |\phi(\boldsymbol{\alpha}(t))\rangle$$

which is called the geometrical phase or Berry phase. This phase can be calculated via the aforementioned time integral, or equivalently by integrating over the curve  $\mathcal{C}$  spanned in the parameter space  $\boldsymbol{\alpha}$  during the adiabatic evolution, reading

$$\gamma_{\mathcal{C}} = \int_{\mathcal{C}} d\boldsymbol{\alpha} \frac{i}{\hbar} \langle\phi(\boldsymbol{\alpha})| \nabla_{\boldsymbol{\alpha}} |\phi(\boldsymbol{\alpha})\rangle \equiv \int_{\mathcal{C}} d\boldsymbol{\alpha} \mathbf{A}(\boldsymbol{\alpha}) \quad [12]$$

with  $\mathbf{A}(\boldsymbol{\alpha})$  the so called Berry connection.

The Berry connection plays the same role in adiabatic evolution as the vector potential in electromagnetism, and indeed, much like in the latter theory, this connection can be used to construct a curvature tensor. In the context of electromagnetism, the curvature tensor is nothing but the electromagnetic tensor  $F_{\mu\nu}$ , while in the context of the adiabatic evolution of quantum systems, it is given the special name of Berry curvature  $\Omega_{\mu\nu}$ . Explicitly, this Berry curvature reads

$$\Omega_{\mu\nu}(\alpha) = \frac{\partial}{\partial\alpha^\mu}A_\nu(\alpha) - \frac{\partial}{\partial\alpha^\nu}A_\mu(\alpha)$$

One often considers the dual pseudo-vector to this tensor, this is  $\Omega_{\mu\nu} = \varepsilon_{\mu\nu\xi}\Omega^\xi$  with  $\varepsilon_{\mu\nu\xi}$  the Levi-Civita symbol, and calls that the Berry curvature instead. This quantity is analogous to the magnetic field  $\mathbf{B} = \nabla \times \mathbf{A}$ . Another similarity between electromagnetism and these concepts is that the Berry connection, like the magnetic vector potential, is defined only up to a gauge choice. This makes it so the Berry phase is only well defined if closed curves  $\mathcal{C}$  in the parameter space are considered.

As a final summary, information about the topology of the target space of  $\mathcal{H}(\alpha)$  is acquired by integrating the Berry connection or curvature over the entire Brillouin zone, or in other words, the holonomy of the Hamiltonian as the Brillouin zone is traversed is sensitive to the band-topology. The integration of this Berry curvature yields quantities called topological invariants which are analogous to the Winding number of the Aharonov-Bohm effect (see the example below). In this  $d > 0$  context, one can also refer to the topological invariants as Chern number.

A fundamental consequence of having a well-defined topological invariant in  $d > 0$  is the so-called bulk-boundary correspondence. This principle asserts that nontrivial topological properties in the bulk of a material inevitably give rise to robust, gapless modes at its boundaries, whether along edges in 2D or surfaces in 3D. One can intuitively see why this should be the case by noting that at the boundary of a topological non-trivial system there is only vacuum, a topological trivial system. This means that, at this boundary, the topological invariant must change from something non-zero to zero which is only possible if the gap closes. This gives rise to emergent gapless edge state which are protected against perturbations that do not close the bulk gap.

## 2. Aharonov-Bohm effect

As a predecessor to the topological band theory, we now introduce the reader to an electromagnetism examples known as the Aharonov-Bohm (A-B) effect as a starting point to understanding the Berry phase, connection, curvature in more detail.

Consider an electron whose movement is restricted to the  $xOy$  place where an infinitely thin and long solenoid pierces through it at its center. Inside the solenoid an electric current flow inducing a magnetic field  $\mathbf{B} = B\hat{z}$  such that a magnetic flux  $\phi$  flows penetrates the the plane of motion of the electron. Although there exists no field or flux outside the solenoid, a magnetic vector potential  $\mathbf{A}$  permeates all space. Now, note that the electron wandering the plane will actually be affected by the vector potential, in that the Hamiltonian describing it will have the form

$$\mathcal{H}(\mathbf{r}) = \frac{\hbar^2}{2m} (\nabla_{\mathbf{r}} - e\nabla_{\mathbf{r}} \cdot \mathbf{A}(\mathbf{r}))^2 \quad [13]$$

with  $\mathbf{p} = -i\hbar\nabla_{\mathbf{r}}$  the momentum operator,  $e$  the electron charge and  $m$  its mass. In this case, the parameters  $\alpha$  can be identified with the actual position of the electron  $\mathbf{r}$ . Since the electron cannot enter the solenoid, which is assumed to be placed at  $\mathbf{r} = 0$ , its movement is restricted to everywhere except there.

As explain in the previous section, as the electron moves following a curve  $\mathcal{C}$  it will acquire a Berry phase, or rather, is in this context, the A-B phase, given by equation [12] as

$$\gamma_{\text{A-B}} = \frac{e}{\hbar} \oint_{\mathcal{C}} d\mathbf{r} \mathbf{A}(\mathbf{r}), \quad [14]$$

with  $\mathbf{A}$  being not the general Berry connection but the actual physical vector potential. The A-B phase, in some sense, measures the inability of making a continuous gauge choice for the magnetic vector potential in a punctured plane. The presence of the puncture hole makes it so a discontinuity along a branch cut is a mathematical necessity, and as a result, if an electron loops around the hole, it will acquire a non-trivial phase, dependent only on the number of times it goes around the hole (see figure [3]). For this reason, it is said that the A-B phase is a topological quantity, depending only on the topology of the electron's trajectory, namely on a quantity called the winding number.

Alternatively, through the usage of Stoke's theorem, it is simple enough to compute the A-B phase as being proportional to the magnetic flux, this is

$$\gamma_{\text{A-B}} = \frac{e}{\hbar} \oint dS \cdot \mathbf{B} = \frac{e}{\hbar} W\phi$$

enclosed by the trajectory's area  $S$ , where  $W \in \mathbb{Z}$  counts the number of loops the electron makes around the solenoid. It's precisely this quantity that corresponds precisely to the winding number.

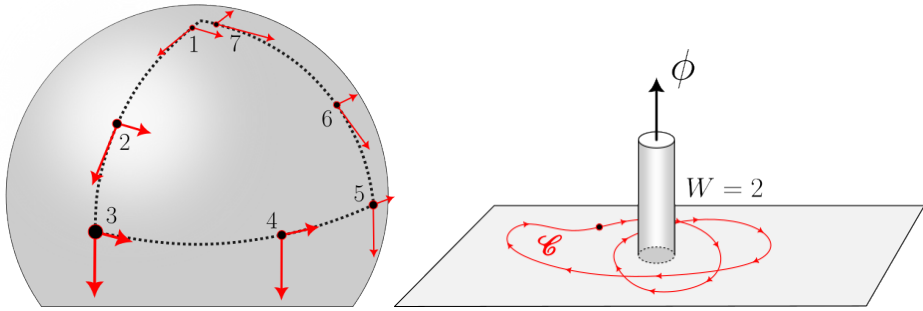


Figure 3. (a) Holonomy, (b) Aharonov-Bohm effect

### 3. Quantum Thouless pump

## II. TOPOLOGICAL SUPERCONDUCTIVITY IN 1D MODELS

### A. Kitaev model

The *Kitaev chain* or *Kitaev-Majorana chain* is a toy model for a topological superconductor using a 1D hybrid (semiconductor+superconductor) nanowires featuring Majorana bound states. It consists of a 1D linear lattice of  $N$  sites and spinless fermions at zero temperature, subjected to nearest neighbor hopping interactions. The real-space tight-binding Hamiltonian describing such model reads

$$H = \mu \sum_{i=1}^N \left( c_i^\dagger c_i - \frac{1}{2} \right) - t \sum_{i=1}^{N-1} \left( c_{i+1}^\dagger c_i + h.c. \right) + \Delta \sum_{i=1}^{N-1} \left( c_{i+1}^\dagger c_i^\dagger + h.c. \right) \quad [15]$$

with  $c_i^\dagger$  ( $c_i$ ) fermionic creation (annihilation) operators,  $\mu$  the chemical potential,  $t$  the hopping energy and  $\Delta$  an proximity induced superconducting  $p$ -wave pairing.

The objective of this model definition is to be able to have a Majorana bound states on the edges mode. For this, let us engineering the Hamiltonian in such a special way that it is actually possible to separate two Majoranas. Foremost, we define each site  $n$  as if it has two sublattices,  $s = A$  and  $s = B$ .

We then define Majorana operators relating to the fermionic operators as

$$\gamma_i^A = c_i^\dagger + c_i \quad \text{and} \quad \gamma_i^B = i(c_i^\dagger - c_i) \quad [16]$$

or rather, in the opposite way, as

$$c_i^\dagger = \frac{1}{2}(\gamma_i^A - i\gamma_i^B) \quad \text{and} \quad c_i = \frac{1}{2}(\gamma_i^A + i\gamma_i^B) \quad [17]$$

Indeed, each site can host a fermion or, equivalently, each site hosting two Majorana modes. These Majorana operators are Hermitian  $\gamma_i^s = (\gamma_i^s)^\dagger$ , unitary  $(\gamma_i^s)^2 = 1$  and anticommute as  $\{\gamma_i^s, \gamma_j^s\} = 2\delta_{ij}\delta_{ss'}$ .

Substituting directly into the Hamiltonian of equation [15] the fermionic operators as given by equations [17] we obtain

$$H = -i\mu \frac{1}{2} \sum_{i=1}^N \gamma_i^B \gamma_i^A + i \frac{1}{2} \sum_{i=1}^{N-1} (\omega_+ \gamma_i^B \gamma_{i+1}^A + \omega_- \gamma_{i+1}^B \gamma_i^A), \quad \text{with } \omega_\pm = \Delta \pm t \quad [18]$$

From it we can distinguish between two phases—trivial and topological—, corresponding, respectively, to two different ways of pairing these Majoranas states—no unpaired modes or one isolated mode on both edges. These pairing configuration are depicted in figure [4] in blue and red respectively. This phases can be easily identified, respectively, in their limiting regimes where one sets  $\Delta = t = 0$  and  $\mu = 0$  with  $\Delta = t \neq 0$ .



Figure 4. Kitaev chain Majorana modes pairing possibilities

Indeed, see that by setting  $\Delta = t = 0$  within the Hamiltonian of equation [18] we obtain

$$H_{\text{trivial}} = -i\mu \frac{1}{2} \sum_{i=1}^N \gamma_i^B \gamma_i^A, \quad [19]$$

which corresponds to the limiting case of "no unpaired Majorana modes" configuration. The energy cost for each fermion to be occupied is  $\mu$ , with all excitations having an energy of either  $\pm\mu/2$ . The band structure will then have a gapped bulk and no zero energy edge states. Furthermore, see that the wavefunctions of the first three energy states shown in figure [5] in this trivial phase simply resemble the harmonic modes of a string states.

On the other hand, see that by setting  $\mu = 0$  with  $\Delta = t \neq 0$  we obtain

$$H_{\text{topological}} = it \sum_{n=1}^{N-1} \gamma_n^B \gamma_{n+1}^A \quad [20]$$

which corresponds to the "unpaired edge Majorana mode" configuration where every Majorana operator is coupled to a Majorana operator of a different kind in the next site. Note that the summation only goes up to  $n = N - 1$ . Moreover, see that by assigning a new fermion operator  $\tilde{c}_i = 1/2(\gamma_i^B + i\gamma_{i+1}^A)$ , the Hamiltonian can be otherwise expressed as

$$H_{\text{topological}} = 2t \sum_{n=1}^{N-1} \left( \tilde{c}_n^\dagger \tilde{c}_n + \frac{1}{2} \right) \quad [21]$$

which describes a new set of  $N - 1$  Bogoliubov quasiparticles with energy  $t$ . For every Majorana pair we assign an energy difference  $2t$  between the empty and filled state. All states which are not at the ends of the chain have an energy of  $\pm t$  and thus the bands structure has a gapped bulk. However, see that the missing mode  $\tilde{c}_N = 1/2 (\gamma_N^B + i\gamma_1^A)$ , which couples the Majorana operators from the two endpoints of the chain, does not appear in the Hamiltonian and thus it most have zero energy. As the presence of this mode does not change the total energy, the ground state is two-fold degenerate. This condition is a topological superconducting non-trivial phase. This mode is called a Majorana zero mode and is highly delocalized at the edges, as it can be seen in red in figure [5]. As one tunes  $\mu$  in the direction of the trivial phase, the topological gap, protected by particle-hole symmetry (PHS), gets smaller and smaller and the Majoranas wavefunctions stay less and less localized at the edges. At the transition between the trivial and topological, when the chemical potential takes it's critical value of  $|\mu| = 2t$ , the first energy states stays evenly distributed along the chain.

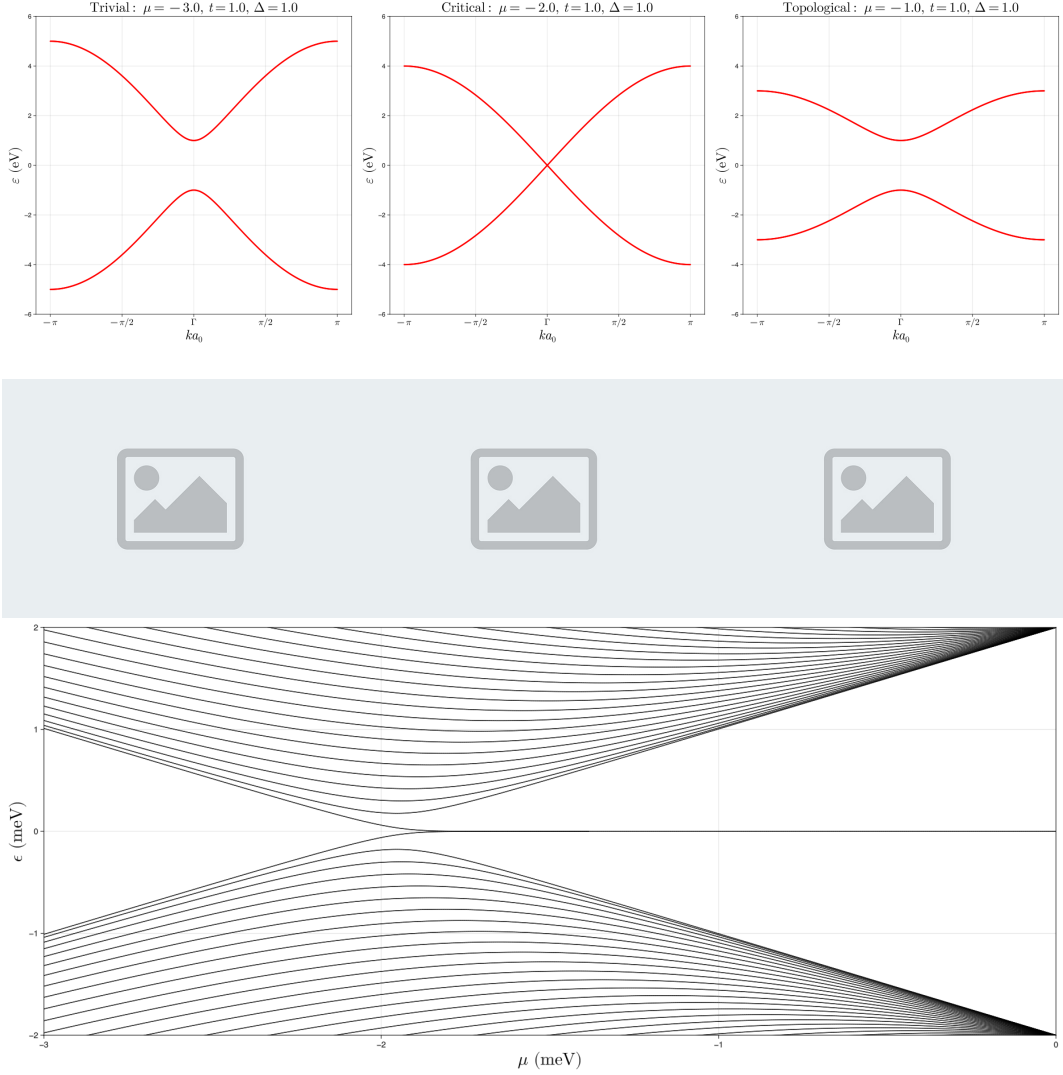


Figure 5. Kitaev chain (top) band structure (middle) I will eventually plot the 1st, 2nd and 3rd state wavefunction here at each regime, and (bottom) band spectrum for a chain length of  $L = 50$  with lattice spacing  $a_0 = 1$  fixing  $\Delta = t = 1.0$ . The critical  $\mu$  shifts forward to infinity as  $L \rightarrow 0$ .

*Bogoliubov-de Gennes Hamiltonian* Let us now define the Hamiltonian in E.(15) in its Bogoliubov-de Gennes (BdG) form

$$H = \frac{1}{2} \check{c}^\dagger H_{\text{BdG}} \check{c}.$$

where we have defined the Nambu spinor as

$$\check{c}_i^\dagger = \begin{pmatrix} c_i^\dagger & c_i \end{pmatrix} \quad \text{and} \quad \check{c}_i = \begin{pmatrix} c_i \\ c_i^\dagger \end{pmatrix} \quad [22]$$

This proves not only useful to the study of the system's symmetries, but it also a necessary step for the numerical implementation in *Quantical.jl*. Defining  $\tau_x, \tau_y, \tau_z$  as Pauli matrices in the particle-hole

subspace and using we the fermionic anti-commutation properties  $\{c_i, c_j^\dagger\} = \delta_{ij}$  and  $\{c_i, c_j\} = 0$ , one can check that

$$\mu : \quad \check{c}_i^\dagger \tau_z \check{c}_i = \begin{pmatrix} c_i^\dagger & c_i \end{pmatrix} \begin{pmatrix} 1 & 0 \\ 0 & -1 \end{pmatrix} \begin{pmatrix} c_i \\ c_i^\dagger \end{pmatrix} = c_i^\dagger c_i - c_i c_i^\dagger = 2c_i^\dagger c_i - 1 \quad [23]$$

$$t : \quad \check{c}_j^\dagger \tau_z \check{c}_i = \begin{pmatrix} c_j^\dagger & c_j \end{pmatrix} \begin{pmatrix} 1 & 0 \\ 0 & -1 \end{pmatrix} \begin{pmatrix} c_i \\ c_i^\dagger \end{pmatrix} = c_j^\dagger c_i - c_j c_i^\dagger = c_j^\dagger c_i + h.c \quad [24]$$

$$\Delta : \quad \check{c}_j^\dagger i \tau_y \check{c}_i = \begin{pmatrix} c_j^\dagger & c_j \end{pmatrix} \begin{pmatrix} 0 & 1 \\ -1 & 0 \end{pmatrix} \begin{pmatrix} c_i \\ c_i^\dagger \end{pmatrix} = c_j^\dagger c_i^\dagger - c_j c_i = c_j^\dagger c_i^\dagger + h.c \quad [25]$$

Hence the Hamiltonian in equation [15] in its BdG form reads as

$$H = \mu \frac{1}{2} \sum_i \check{c}_i^\dagger \tau_z \check{c}_i - t \sum_{i=1}^{N-1} \check{c}_{i+1}^\dagger \tau_z \check{c}_i + \Delta \sum_{i=1}^{N-1} \check{c}_{i+1}^\dagger i \tau_y \check{c}_i \quad [26]$$

See that the Hamiltonian has particle-hole symmetry, i.e  $\mathcal{P} H \mathcal{P}^{-1} = -\tau_x H^* \tau_x = -H$  with  $\mathcal{P} = \tau_x \mathcal{K}$  and  $\mathcal{K}$  complex conjugation, as well as time reversal symmetry, i.e  $\mathcal{T} H \mathcal{T}^{-1} = H^* = H$  with  $\mathcal{T} = \mathcal{K}$  for this spinless case (for reference,  $\mathcal{T} = i\sigma_y \mathcal{K}$  for a 1/2-spin system). Once again, to understand why this is the case check.

### Topological invariant

#### 1. Majorana modes at a domain wall

Consider the case where we weld together two semi-infinite nanowires with one in it's trivial phase and the other in it's trivial phase. The spacial profile of the chemical potential  $\mu(x)$  would then approximately a Heaviside theta function from  $|\mu_{\text{left}}| > 2t$  to  $|\mu_{\text{right}}| < 2t$ , forming a doping domain wall at it's center. Hamiltonian wise, one just substitutes  $\mu \rightarrow \mu(x)$  directly into equation [15]. What one obtains in this situation is a Majorana mode localized at the domain wall with its twin forming in the semi-infinite edge of the topological side.

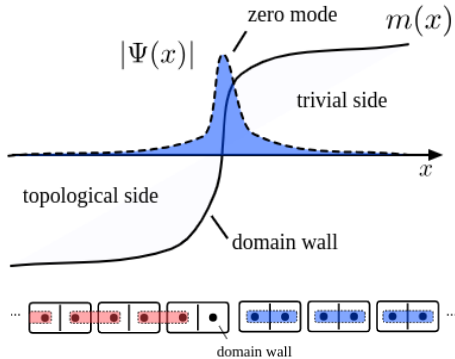


Figure 6. needs caption

### 2. Kitaev ring

#### 3. Doublet Kitaev chain

#### B. SSH model

The most relevant references used for this section follow:

#### C. Oreg-Lutchyn models

I found some good intuitive remarks on Stoudenmire 2011 PRB which eventually I wish to include.

The Oreg-Lutchyn Majorana minimal model consists of a finite 1D semiconductor (SM) nanowire with strong spin-orbit coupling (SOC)  $\alpha$  and a tunable chemical potential  $\mu$ , in proximity of a superconductor (SC) of homogeneous pairing  $\Delta$ , having a magnetic field  $B_z$  applied along its length, defined as the  $\hat{z}$  direction. The Rashba effect describes the coupling of an electric field  $E_x$  that breaks inversion symmetry breaking in the direction perpendicular to the wire, to the electron's spin, i.e  $\propto (i\vec{\nabla} \times \hat{x}) \cdot \vec{\sigma} = i\sigma_y \partial_z$  with  $\vec{\sigma} = (\sigma_x, \sigma_y, \sigma_z)$ . The Zeeman effect described the spin splitting due to the in-plane magnetic field  $B_z$ . The pairing term describes the Cooper pairs from BCS theory than could tunnel from the SM to the SC.

The tight-binding Hamiltonian describing such system can then be decomposed as

$$H = H_K + H_{SOC} + H_Z + H_{SC} \quad [27]$$

$$H_K = (2t - \mu) \sum_{i\sigma} c_{i\sigma}^\dagger c_{i\sigma} - t \sum_{\langle i,j \rangle \sigma} c_{i\sigma}^\dagger c_{j\sigma} \quad [28]$$

$$H_{SOC} = \frac{\alpha}{2a_0} \sum_{i\sigma} (c_{i+1\bar{\sigma}}^\dagger c_{i\sigma} + h.c.) \quad [29]$$

$$H_Z = V_Z \sum_i (c_{i\uparrow}^\dagger c_{i\uparrow} - c_{i\downarrow}^\dagger c_{i\downarrow}) \quad [30]$$

$$H_{SC} = \Delta (c_{i\downarrow}^\dagger c_{i\uparrow}^\dagger + h.c.) \quad [31]$$

with  $c_i^\dagger$  ( $c_i$ ) fermionic creation (annihilation) operators,  $\mu$  the chemical potential,  $t = \eta/a_0^2$  the hopping energy into  $\langle i, j \rangle$  nearest-neighbouring sites with  $a_0$  the lattice constant and  $\eta = \hbar^2/2m^*$  with  $m^*$  the effective mass of the electrons,  $V_Z = g_J \mu_B B_z / 2$  the Zeeman potential with  $g_J$  the Landé gyromagnetic moment and  $\mu_B$  Bohr's magneton,  $\alpha$  the Rashba SOC strength and  $\Delta$  proximity induced superconducting  $s$ -wave pairing.

A paragraph explaining the bands.

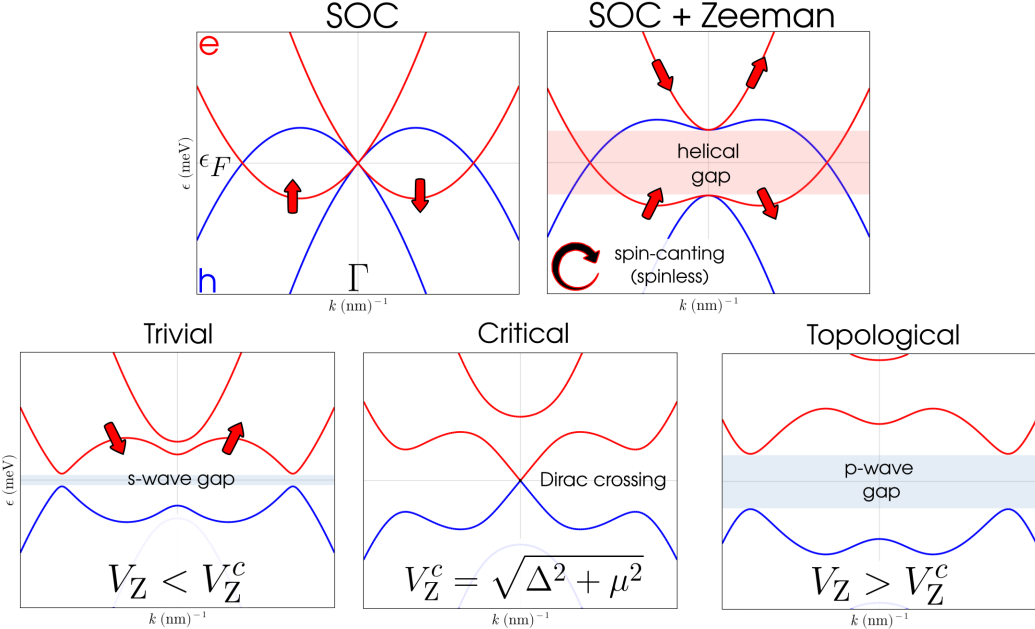


Figure 7.

A paragraph explaining the phase-diagram, pfaffian and band spectrum.

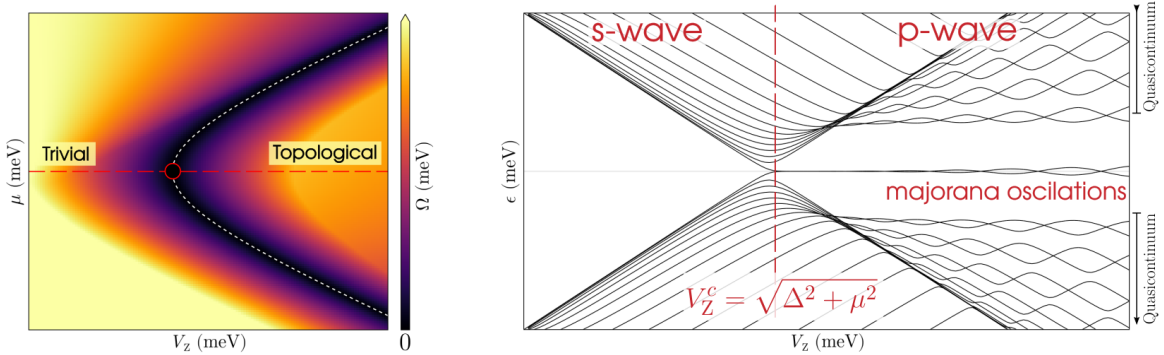


Figure 8.

*Bogoliubov-de Gennes Hamiltonian* Shown below are the broad strokes of a numerical implementation of the Hamiltonian in Julia using the Quantica.jl. However, prior to this implementation, we will be needing the Bogoliubov-de Gennes formalism. For this, need to double the degrees of freedom through the Nambu-spinor. In the so called unrotated-spin basis we define a Nambu spinor as

$$\check{c}_i^\dagger = \begin{pmatrix} c_i^\dagger & c_i \end{pmatrix} = \begin{pmatrix} c_{i\uparrow}^\dagger & c_{i\downarrow}^\dagger & c_{i\uparrow} & c_{i\downarrow} \end{pmatrix} \quad [32]$$

In this Nambu $\otimes$ spin orbital space the Hamiltonian in equation [27] reads

$$H = H_K + H_{SOC} + H_Z + H_{SC} \quad [33]$$

$$H_K = (2t - \mu) \sum_i \check{c}_i^\dagger [\tau_z \otimes \sigma_0] \check{c}_i - \frac{1}{2} t \sum_{\langle i,j \rangle} \check{c}_i^\dagger [\tau_z \otimes \sigma_0] \check{c}_j \quad [34]$$

$$H_{SOC} = \frac{\alpha}{2a_0} \sum_i \check{c}_i^\dagger [\tau_z \otimes i\sigma_y] \check{c}_{i+1} \quad [35]$$

$$H_Z = V_Z \sum_i \check{c}_i^\dagger [\tau_z \otimes \sigma_z] \check{c}_i \quad [36]$$

$$H_{SC} = \frac{1}{2} \Delta \sum_i \check{c}_i^\dagger [\tau_y \otimes \sigma_y] \check{c}_i \quad [37]$$

with  $\tau$  Pauli matrices in the particle-hole subspace and  $\sigma$  in the spin subspace.

To understand why this is the case check we show explicitly the derivation for the pairing term as an example. It reads:

$$\begin{aligned} \check{c}^\dagger [\tau_y \otimes \sigma_y] \check{c} &= \left( \begin{array}{cccc} c_\uparrow^\dagger & c_\downarrow^\dagger & c_\uparrow & c_\downarrow \end{array} \right) \left( \begin{array}{cc|cc} 0 & 0 & 0 & -1 \\ 0 & 0 & +1 & 0 \\ \hline 0 & +1 & 0 & 0 \\ -1 & 0 & 0 & 0 \end{array} \right) \left( \begin{array}{c} c_\uparrow \\ c_\downarrow \\ c_\uparrow \\ c_\downarrow \end{array} \right) \\ &= -c_\uparrow^\dagger c_\downarrow^\dagger + c_\downarrow^\dagger c_\uparrow^\dagger + c_\uparrow c_\downarrow - c_\downarrow c_\uparrow = 2 (c_\downarrow^\dagger c_\uparrow^\dagger + \text{h.c.}) \end{aligned} \quad [38]$$

where we the fermionic anti-commutation properties  $\{c_i, c_j^\dagger\} = \delta_{ij}$  and  $\{c_i, c_j\} = 0$ .

The remaining terms derivation is analogous but even simpler because there is will be no mixing of particle with particle-hole components; the holeonic terms will correspond to the negative of the electronic terms, meaning that one just needs to expand the space according to  $\tau_z \otimes$  the respective spin matrix. For the kinetic term there is no mixing of spin so it must trivially have the spin Pauli matrix  $\sigma_0$ . Similarly, for the Zeeman term there is only the same-spin mixing of the type  $\uparrow\uparrow - \downarrow\downarrow$  so it must have  $\sigma_z$ . As for the SOC term there is spin-mixing of opposing spins, so the options are either  $\sigma_x$  or  $i\sigma_y$  (with a  $i$  for it to be hermitian). One can check with the fermionic anti-commutation properties that it is indeed  $i\sigma_y$ .

*Alternative Nambu basis* It is common for people to define instead the Nambu spinor in a rotated basis as such

$$\bar{c}_i^\dagger = \left( \begin{array}{c} c_i^\dagger \\ [i\sigma_y c_i] \end{array} \right) = \left( \begin{array}{cc} c_{i\uparrow}^\dagger & c_{i\downarrow}^\dagger \\ \hline c_{i\downarrow} & -c_{i\uparrow} \end{array} \right) \quad [39]$$

As also explained in section II.C.1 of the previous part, these basis' operators relate to each other as

$$\bar{c}_i = \bar{\mathcal{U}} \check{c}_i \Leftrightarrow \check{c}_i = \bar{\mathcal{U}}^\dagger \bar{c}_i \quad [40]$$

$$\bar{c}_i^\dagger = \check{c}_i^\dagger \bar{\mathcal{U}}^\dagger \Leftrightarrow \check{c}_i^\dagger = \bar{c}_i^\dagger \bar{\mathcal{U}} \quad [41]$$

and, consequently, for a generic  $\check{M}$  matrix,

$$\bar{M} = \bar{\mathcal{U}} \check{M} \bar{\mathcal{U}}^\dagger \quad [42]$$

with  $\bar{\mathcal{U}}$  is a unitary matrix (i.e  $\bar{\mathcal{U}}^\dagger \bar{\mathcal{U}} = \bar{\mathcal{U}} \bar{\mathcal{U}}^\dagger = \mathbb{1}$ )

$$\bar{\mathcal{U}} = \begin{pmatrix} \sigma_0 & 0 \\ 0 & \imath\sigma_y \end{pmatrix} \quad [43]$$

Making use of Pauli matrices' property

$$\sigma_\alpha \sigma_\beta = \sigma = \sigma_0 \delta_{\alpha\beta} + i \varepsilon_{\alpha\beta\gamma} \sigma_\gamma \quad [44]$$

one can check that

$$H_K : \bar{\mathcal{U}} [\tau_z \otimes \sigma_0] \bar{\mathcal{U}}^\dagger = [\tau_z \otimes \sigma_0] \quad [45]$$

$$H_{SOC} : \bar{\mathcal{U}} [\tau_z \otimes \imath\sigma_y] \bar{\mathcal{U}}^\dagger = [\tau_z \otimes \imath\sigma_y] \quad [46]$$

$$H_Z : \bar{\mathcal{U}} [\tau_z \otimes \sigma_z] \bar{\mathcal{U}}^\dagger = [\tau_z \otimes \sigma_z] \quad [47]$$

$$H_{SC} : \bar{\mathcal{U}} [\tau_y \otimes \sigma_y] \bar{\mathcal{U}}^\dagger = [\tau_x \otimes \sigma_0] \quad [48]$$

meaning that, in this the rotated basis, only the pairing Hamiltonian has it's Pauli matrices changed.  
Concretely,

$$H_{SC} = \frac{1}{2} \Delta \sum_i \bar{c}_i^\dagger [\tau_x \otimes \sigma_0] \bar{c}_i \quad [49]$$

### III. TOPOLOGICAL SUPERCONDUCTIVITY IN 2D MODELS

Need a intuitive and organized introduction relating all the nomenclatures "topological insulator", "Chern insulator" with the various effects. I still don't have a clear map of what's what and the subtle symmetry differences.

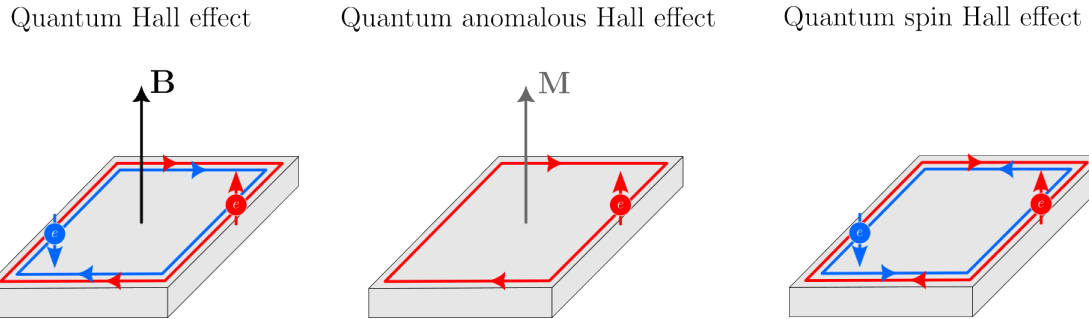


Figure 9. Members of the Hall family.  $\mathbf{B}$  is an external magnetic field,  $\mathbf{M}$  an intrinsic spontaneous magnetization, and the electron arrows denotes spin. Say which symmetries are being broken in each case. Time-reversal, time-reversal and spacial invariance symmetry, and ????. And maybe I prefer to put the images being the actual examples I give, corbino disk, zigzag graphene and ???

#### A. Integer quantum hall effect

##### 1. Classical Hall effect and Landau quantization

###### *Classical Hall effect*

Let us begin by considering the classical Hall effect. In this well-known phenomenon, an electric

current is established along the  $x$  axis of a conductive material. A magnetic field is then applied perpendicular to the current, typically oriented along the  $z$  axis, that is, normal to the plane of the conductor. This configuration gives rise to the Lorentz force, which acts on the charge carriers and deflects them in the  $y$  direction. The Lorentz force, given by  $\mathbf{F} = e(\mathbf{v} \times \mathbf{B})$ , arises from the interaction between the charge carrier's motion and the applied magnetic field, with  $e$  and  $\mathbf{v}$  the charge and velocity vector of the carriers, and  $\mathbf{B}$  the magnetic field. This deflection results in an accumulation of charge on opposite edges of the conductor, which induces a transverse electric field. Eventually, this electric field balances the Lorentz force, preventing further charge separation. The resulting potential difference across the  $y$  axis is known as the Hall voltage. Since the transverse electric field arises specifically to counteract the Lorentz force, which is itself proportional to the strength of the applied magnetic field, it follows that the Hall voltage is expected to vary linearly with the magnetic field. Consequently, the Hall resistivity, defined as the ratio of the Hall voltage to the current, is likewise expected to exhibit a linear dependence on the magnetic field. These concepts and quantities are depicted in figure [10].

Prior to the discussion of the quantum Hall effect, let us make some addition "back-of-the-envelope calculations" to gain a better intuition of the problem at hand.

#### *Streda relation*

Let us posit the ansatz that the electrons enter a steady state. Such a steady state can be obtained by making a Galilean transformation to a reference frame moving with velocity  $\mathbf{v}$  with respect to the original reference frame. In this steady state the average force on the electrons must be zero,  $\mathbf{F} = e(\mathbf{E} + \mathbf{v} \times \mathbf{B}) = 0$ . The corresponding current density, defined as  $\mathbf{j} = ne\mathbf{v}$  with  $n$  the electron density, can then be expressed as  $\mathbf{j} = (ne/B)(\mathbf{E} \times \mathbf{z})$ . In terms of conductance one can write  $\mathbf{j} \equiv \sigma_H(\mathbf{E} \times \mathbf{z})$  with  $\sigma_H = ne/B$  the so-called Hall conductance or Streda relation. Moreover, if we define the so-called "filling factor" as  $\nu = nh/(eB)$  the Hall conductance can then be written as a multiple of the quantum of conductance as

$$\sigma_H = \nu e^2/h. \quad [50]$$

At relatively high carrier densities, the Hall conductivity behaves in accordance with the classical expression above, and it typically scales linearly with gate voltage, which tunes the electron density  $n$ . However, at low filling factors, the situation becomes more intricate. One might reasonably expect that various non-idealities such as disorder, lattice effects, or electron-electron interactions would violate the assumptions underlying Galilean invariance. As a result, deviations from the simple linear dependence of  $\sigma_H$  could arise, leading to sample-specific behavior that is sensitive to microscopic details.

#### *Landau quantization*

Let us now examine the Schrödinger equation for an ideal 2D electron gas subject to a perpendicular magnetic field. The system is then described by the Hamiltonian  $H(\mathbf{r}) = \frac{1}{2m}(\mathbf{p} - e\mathbf{A}(\mathbf{r}))^2$  with  $\mathbf{p}$  the canonical momentum operator and  $\mathbf{A}(\mathbf{r})$  the vector potential operator. A convenient gauge choice in this context is one in which the vector potential, related to the externally-applied uniform magnetic field  $\mathbf{B} = B\mathbf{z}$  as  $\mathbf{B} = \nabla \times \mathbf{A}$ , depends only on the  $y$ -coordinate, concretely  $\mathbf{A}(x, y) = \hat{\mathbf{x}}By$ . In this gauge, known as Landau gauge, the Hamiltonian reads instead as

$$H(\mathbf{r}) = \frac{p_x^2}{2m} + \frac{1}{2}m\omega_c^2 \left( x - \frac{\hbar k_y}{m\omega_c} \right)^2, \text{ with } \omega_c = eB/m \quad [51]$$

the cyclotron frequency. See that, since the operator  $y$  is absent for this choice of gauge, the operator  $p_y$  commutes with the Hamiltonian meaning that this form is translationally invariant along the  $y$ -direction. This allows us to replace  $p_y$  by its eigenvalue  $\hbar k_y$ , identifying  $k_y$  as a good quantum number. Apart from a shift of the  $x$ -coordinate by an amount  $x_0(k_y) = \hbar k_y/m\omega_c$ , the resulting Hamiltonian corresponds to that of a 1D quantum harmonic oscillator. Consequently, the eigenenergies of this system are thus identical to those of the standard quantum harmonic oscillator, given by

$$E_n = \hbar\omega_c \left( n + \frac{1}{2} \right). \quad [52]$$

The corresponding wave functions, due to the commutation relation  $[p_y, H] = 0$ , will then factor into a product of plane-waves in the  $y$ -direction and shifted harmonic oscillator eigenstates, this is  $\psi(\mathbf{r}) = e^{ik_y y} \phi_n(x - x_0)$ . Each collection of states associated with a fixed quantum number  $n$  defines a so-called Landau level.

To understand the degeneracy of these Landau levels, let us consider the physical constraints of the system. These discrete energy levels become observable only when the thermal energy  $k_B T$  is smaller than the level spacing  $\hbar\omega_c$ , which places us in the regime of low temperatures and strong magnetic fields. Within this regime, each Landau level is highly degenerate, as the quantum number  $k_y$  may take values  $k_y = 2\pi N/L_y$  with  $N$  an integer and  $L_y$  the system's length in the  $y$ -direction. Moreover, the allowed values of  $N$  are further restricted by the condition that the center of force of the oscillator must physically lie within the system, i.e  $0 \leq x_0 < L_x$ , with  $L_x$  the system's length now in the  $x$ -direction. Because of this,  $N$  must range between zero and  $m\omega_c A/2\pi\hbar$ , with  $A = L_x L_y$  the total area of the system. For electrons, spin-1/2 particles of elemental charge, this upper bound on  $N$  can be further expressed in terms of the ratio  $N_{\max} = 2\Phi/\Phi_0$ , with  $\Phi_0 = h/e$  the fundamental magnetic flux quantum and  $\Phi = BA$  the flux through the system. This result means that each Landau level can accommodate exactly two electrons per flux quantum that penetrates the system. If, for example, Zeeman splitting is included, each Landau level would split into a pair, one for spin up electrons and the other for spin down electrons, with the occupation of each spin Landau level being just one electron (per flux quantum). In the spinless case, if  $n$  Landau levels are filled at a given chemical potential, the filling factor must be  $\nu = n$ , which, by Streda formula's, leads directly to the Hall conductance

$$\sigma_H = ne^2/h. \quad [53]$$

## 2. Quantum Hall chiral edge states

As we just discussed, for clean two-dimensional electronic systems at low temperatures, the Hall voltage initially exhibits a linear dependence on the applied magnetic field, as predicted by classical theory. However, as the magnetic field increases further, this linear trend breaks down and distinct plateaus emerge in the Hall voltage, as seen in figure [10]. This phenomenon is known as the quantum Hall effect, first discovered in two-dimensional electron gases subjected to low temperatures and strong magnetic fields. More remarkably, the Hall resistivity becomes quantized, taking on discrete values given by  $R_H = h/(e^2\nu)$  with  $h$  the Planck's constant and  $\nu$  an integer known as the filling factor. This quantization is extraordinarily precise—accurate to more than one part in a billion—and is observed universally, regardless of the microscopic details of the material, the geometric shape of the sample, or even variations in sample purity. The robustness and universality of this quantization reflect the topological nature of the quantum Hall effect since it arises from global properties rather than local perturbations. In this context, the filling factor is the topological invariant characterizing the system.

Let us inspect once more figure [10]. Observe that, accompanying the quantization of the Hall resistivity, the longitudinal resistivity appears to vanish within the plateau regions. This implies that during these quantized regimes there is effectively no dissipation of electrical energy along the direction of current flow, indicating that the electric field and the current density are orthogonal to each other. In other words, the current flows entirely transverse to the applied electric field, a hallmark of purely Hall-type conduction. This orthogonality is a direct consequence of the topological nature of the quantum Hall state, in which extended edge states carry current without back-scattering, while the bulk of the material remains insulating. This insulating behavior of the bulk is further corroborated by the  $\exp(-T_0/T)$  temperature dependence of the longitudinal transport coefficients behavior. This characteristic thermal activation implies that charge transport in the bulk is suppressed at low temperatures, indicating the presence of an energy gap which must be overcome for carriers to contribute to conduction. However, in the quantum Hall regime—as in all topological phases of matter—a crucial distinction arises. The energy gap does not extend uniformly across the entire system. Instead, it necessarily vanishes at the edges of the sample as stated by the bulk-edge correspondence.

### *Additional remarks*

An alternative and intuitive justification for the existence of chiral edge states arises from a semiclassical perspective. Consider the classical trajectory of an electron moving with velocity  $\mathbf{v}$  in a uniform magnetic field  $\mathbf{B}$  perpendicular to the plane of motion. In such a scenario, the electron follows a circular trajectory known as a cyclotron orbit, with radius given by  $r_c = mv/eB$ . Furthermore, the angular momentum of an electron undergoing this motion is  $L = mvrc = eBr_c^2$ . In the quantum mechanical framework, angular momentum is quantized, so only orbits satisfying  $L = n\hbar$  with  $n \in \mathbb{N}$  are permitted. Equating this with the classical expression yields  $r_c^2 = n\hbar/eB$ , implying that the allowed cyclotron radii are discrete and given by  $r_n = \sqrt{n}l_B$  with  $l_B = \sqrt{\hbar/eB}$  the so-called the magnetic length. Moreover, all such orbits, regardless of radius, rotate at the same cyclotron frequency  $\omega_c = eB/m$ . As a result, the energy associated with the quantized circular motion becomes  $E_n = L\omega_c = n\hbar\omega_c$ . Thus, from this semiclassical approach based on angular momentum quantization, we once again recover the same energy spectrum as that of the Landau levels, originally obtained through the analysis of the 1D quantum harmonic oscillator Hamiltonian in Landau's gauge.

Let us now examine the behavior of the classical trajectory of an electron when the center of its cyclotron orbit lies closer to the edge of the sample than the cyclotron radius. In realistic systems, electrons are confined by an electrostatic potential that prevents them from escaping the physical boundaries of the material. As illustrated in figure [10], for the simplest example of a ribbon geometry, the interplay between this confining potential and the strong perpendicular magnetic field modifies the nature of the electron motion near the edges. Instead of executing closed cyclotron orbits, electrons near the boundary are reflected by the potential and trace out open trajectories along the edge, known as skipping orbits. In such configurations, the motion becomes unidirectional: on the lower edge, electrons propagate exclusively to the left, while on the upper edge they move only to the right. Hence, each edge supports states that move in a single direction, with the propagation direction at opposite edges being reversed. These boundary modes are referred to as chiral edge states and their chirality is determined by the direction of the magnetic field perpendicular to the plane of motion. Reversing the magnetic field orientation reverses the direction of propagation at both edges.

The precise shape of the confining potential is not essential for our purposes, provided it satisfies certain generic features. Specifically, it should be approximately flat in the central region of the ribbon, allowing us to set  $V(x_{\text{bulk}}) = 0$ , and should rise steeply near the physical boundaries in order to effectively confine the electrons. As previously discussed, in the bulk of the system, the electron states correspond to classical cyclotron orbits, and the energy spectrum consists of flat Landau levels with energies  $E_n$  that are independent of  $k_y$ . However, states localized within a few magnetic lengths of the edge are significantly affected by the rising confining potential, which in this regime cannot be neglected. Particularly, for states centered at position  $x_0 = \hbar ck/eB$ , the energy is expected to increase by an amount proportional to  $V(x_0)$  with respect to the original Landau level, since  $x_0$  is directly proportional to  $k$ . As depicted in figure [10], the resulting bending of the Landau levels implies that, even when the Fermi level lies in the middle of a bulk gap, there will be energy bands intersecting it, corresponding to the energy of the chiral edge states. Those crossing at negative  $k$  are localized near the lower edge, while those crossing at positive  $k$  are localized near the upper edge. Also, see that, for each edge there are as many edge states as there are filled Landau levels in the bulk of the system.

Moreover, near the Fermi energy, the dispersion of these edge states can be well approximated as linear, yielding a relation of the form  $E = \hbar v(k - k_F)$ , with  $k_F = 2\pi N/L_x$  the Fermi momentum,  $N$  the number of electrons and  $L_x$  the length of ribbon along the  $x$ -direction. Because the slope of the potential is just the local electric field perpendicular to the edge of the sample, the velocity of the edge states can be simply interpreted as the drift velocity of a skipping state, i.e  $v_{\text{edge}} = -\partial_y V(y)/B$ . One can then see that the velocity is opposite at the two edges because the local electric field created by the confining potential always points towards the interior of the sample.

### 3. Non-interacting electrons in a Corbino disk

To understand the quantum Hall bulk-edge correspondence more concretely, let us consider a two-dimensional annular system threaded by an external magnetic flux  $\Phi$ , as illustrated in figure [10]. As the magnetic flux is gradually increased, Faraday's law implies the emergence of an azimuthal electric field. This, in turn, induces a radial current that redistributes charge between the inner and outer edges of the annulus, effectively polarizing the system. In a conventional metallic system, such a redistribution would relax over time due to finite longitudinal conductivity in the bulk, allowing charge to flow back and neutralize the polarization. However, in the quantum Hall regime, the bulk lacks longitudinal conductivity due to the presence of an energy gap. As a result, the induced charge cannot relax through bulk conduction and instead accumulates at the edges. However, for this accumulation to occur, there must exist accessible electronic states near the chemical potential at the edges where the charge can reside. In the regime where the induced electric field is slowly-varying, i.e., of low frequency and with a wavelength on the order of the system size, then the perturbation will not have enough energy to excite carriers across the bulk energy gap, meaning that the only way the system can respond is if zero-energy states are available at the edge. It is important to note that the charge localized at the edge is not conserved. If one "peels off" the outer edge of the sample the resulting structure will just be a thinner annulus, still supports gapless edge states at its new boundaries. This recursive property illustrates that the presence of edge states is not tied to a specific physical location, but rather to the mere existence of a boundary separating the topologically nontrivial quantum Hall bulk from a trivial vacuum.

Another, distinctly quantum mechanical, key ingredient of the system is the requirement that the energy spectrum of the annular system must be periodic with respect to the magnetic flux  $\Phi$  threaded through its hole, with a period equal to one flux quantum,  $\Phi_0 = h/e$ . This is a manifestation of the Aharonov–Bohm effect, as discussed in section [??]. Suppose the system is initially in its ground state with zero flux threading the hole. If we then adiabatically increase the flux to one flux quantum  $\Phi_0$ , the system will remain in an eigenstate due to the slow, coherent nature of the evolution. However, it will generally not return to its original ground state. This is because, during the flux insertion, charge is transferred from one edge of the annulus to the other, leading to a final state with different edge charge distribution. Although this new state is an eigenstate of the system's Hamiltonian, it is not the ground state, due to the energetic cost associated with the imbalance in edge charge. This behavior is completely general and does not depend on microscopic details of the system—it relies solely on the fact that the system is in a topologically nontrivial quantum Hall phase.

Let us now restrict our attention to non-interacting electrons, deferring the discussion of interactions to a later stage in the course. In the non-interacting picture, the many-body eigenstates of the system can be constructed from single-particle states, each of which can be either occupied or unoccupied. At zero temperature, the ground state corresponds to a configuration in which all single-particle states below the chemical potential are filled, while those above remain vacant. Excited states arise when electrons are promoted to higher-energy unoccupied states, leaving vacancies behind. In the quantum Hall regime, since the only eigenstates available at low energy are at the edge, turning on one flux quantum must result in a transfer of an *integer* number of electrons between the edges. This observation leads directly to the quantization of the Hall conductivity: the amount of charge transferred per flux quantum is quantized in integer units of  $e$ , and therefore the Hall conductivity must be quantized in units of  $e^2/h$ .

Note, however, a slight complication on our integer argument. Integers, by their very nature, cannot change continuously. This implies that some aspect of our argument must break down in the regions of magnetic field lying between two quantized Hall plateaus. Indeed, experimental data reveal exactly what goes wrong. In these intermediate regimes, the Hall conductivity is no longer quantized and the longitudinal conductivity becomes non-zero. This indicates that during the adiabatic insertion of magnetic flux, a current still flows from the inner to the outer edge of the sample. However, once the flux insertion is halted, the accumulated edge charge does not remain stable; instead, it relaxes, and

energy is dissipated within the bulk of the system. As a result, the system returns to its original state, signaling the breakdown of perfect quantized transport. Most importantly, see that the emergence of a non-zero longitudinal conductivity signals the closing of the bulk energy gap. As we have emphasized throughout, topological invariants, such as the quantized Hall conductivity, are well-defined only in the presence of a finite energy gap. Therefore, a transition between distinct quantized values must be accompanied by the closure of this gap, allowing the system to change its topological character. In other words, topological numbers are stable under smooth deformations of the Hamiltonian so long as the gap remains open, and can only change when the gap vanishes. This is a general and robust feature of topological phases.

#### *Disclaimer and teaser*

To conclude, we note a brief disclaimer and a teaser. The disclaimer is that, for the sake of clarity, certain complexities have been glossed over, some of which will be addressed later. So far, we have focused on one particular realization of the quantum Hall effect, that of electrons occupying Landau levels. However, many other realizations exist. For example, electrons may experience a periodic potential alongside a magnetic field, and one may include disorder to better represent real physical systems. In these cases, Landau levels are no longer the appropriate single-particle eigenstates, and discussing the new resulting eigenstates is not, in every way, trivial. Rather than delve into these complexities, our focus stayed on the key topological feature, that our topological invariants — the quantized Hall conductivity, quantized Hall resistivity, and robust edge states — remain unchanged as long as the energy gap of the system does not close. The teaser concerns the upcoming discussion of the fractional quantum Hall effect. When the Hall conductivity takes fractional values, for instance  $1/3e^2/h$ , the adiabatic insertion of a single flux quantum into the annulus results in an eigenstate where the exterior edge accumulates a fractional charge equal to one-third of an electron, and the interior accumulates a corresponding fractional hole. This eigenstate is exceptionally stable and effectively persists indefinitely, featuring localized fractional charge, which is a defining characteristic of strongly correlated topological phases. These fascinating phenomena will be explored later, although, as with all topics in this book, the treatment will be introductory and will not cover much details. The goal is instead to provide new readers with a clear understanding of the key concepts and underlying intuitions.

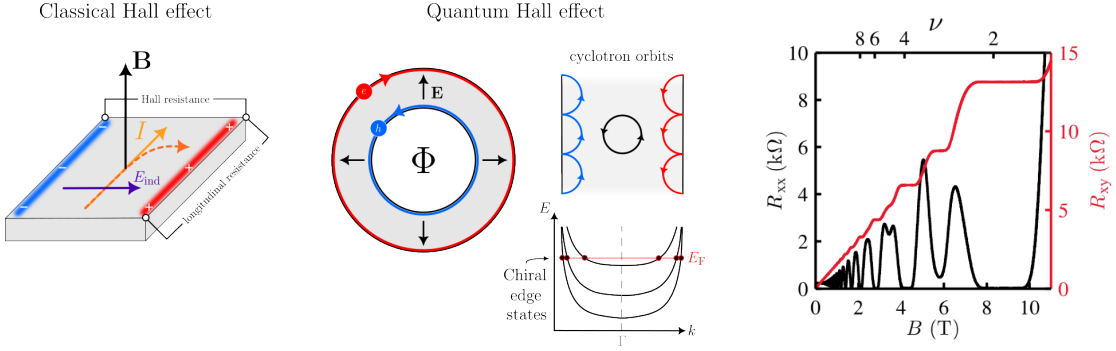


Figure 10. Hall effect. Needs caption.

## B. Anomalous quantum Hall effect

In this section, we demonstrate that the quantum Hall effect can occur even in the absence of strong magnetic fields. In particular, we show that it can arise from a conventional Bloch band structure with broken time-reversal symmetry, yet without any net magnetic flux through the system. This phenomenon is known as the quantum anomalous Hall effect, and it characterizes what are referred to

as Chern insulators. The model discussed in this section, Haldane's graphene model, is widely regarded as a precursor to modern time-reversal invariant topological insulators.

### 1. Graphene's discrete symmetries

As a preliminary note, we recommend that the reader review the basics of graphene, which can be found in appendix [??]. This will provide useful context, as we now turn to discussing graphene from the perspective of its discrete symmetries.

As discussed in appendix [??], graphene is a semi-metal characterized by two inequivalent Dirac points located at the corners of the Brillouin zone, commonly labeled as the  $K$  and  $K'$  points. At these points, the conduction and valence bands meet, and the low-energy excitations are effectively described by a two-dimensional massless Dirac equation. The aim of this section is to examine the topological nature of these gapless Dirac points and the role of symmetry in protecting them. In particular, we discuss that their stability relies on the simultaneous presence of spatial inversion and time-reversal symmetry. If either of these symmetries are broken, the gap will open up.

Starting with the discussion on inversion symmetry, we refer to the operation that exchanges the  $A$  and  $B$  sublattices through a reflection across the horizontal plane that bisects the unit cell, as illustrated in light gray in figure [??]. Given graphene's lattice, this spatial inversion symmetry is intimately connected to sublattice symmetry. Consequently, the Hamiltonian becomes block off-diagonal in the sublattice basis and satisfies the relation

$$\tau_z H(-\mathbf{k}) \tau_z = -H(\mathbf{k}) \quad [54]$$

with  $\tau_z$  the Pauli- $z$  matrix acting in sublattice space. It is important to note, however, that this sublattice symmetry is only approximate. It arises from the idealized tight-binding model limited to nearest-neighbor hopping. If longer-range hoppings were included, both spatial inversion and sublattice symmetries would be explicitly broken. Moreover, as also discussed in appendix [??], these symmetries may also be broken if the  $A$  and the  $B$  sites are occupied by different atoms, as in the case of a gapped semiconductor like hexagonal boron nitride (hBN). Additionally, see that the honeycomb lattice will also possess a three-fold rotational symmetry about the center of the unit cell. While this symmetry is essential for the emergence of Dirac cones in the band structure, it does not influence the mechanism responsible for opening a topological gap.

Regarding time-reversal symmetry invariance, one needs first to note that we take the electrons to be spinless, meaning that they are fully spin-polarized. Since we are neglecting the electron's spin degree of freedom, the time-reversal symmetry operator reduces to a simple complex conjugation, and thus

$$H(\mathbf{k}) = H^*(-\mathbf{k}).$$

See that time-reversal symmetry exchanges the two Dirac cones by mapping  $\mathbf{K}$  into  $-\mathbf{K}'$ . The combination of time-reversal symmetries with the (approximate) sublattice symmetry will then yield a particle-hole symmetry, expressed as

$$\tau_z H^*(-\mathbf{k}) \tau_z = -H(\mathbf{k})$$

### 2. Haldane's graphene model and chirality

The main objective of this section is to demonstrate how graphene can be driven into a quantum Hall state, marked by the presence of chiral edge modes. The first crucial step, common across the broader topological framework, is to open an energy gap in the bulk spectrum. According to the bulk-boundary

correspondence, such a gap implies the emergence of robust edge states at zero energy. As previously discussed, opening a gap at the Dirac points  $K$  and  $K'$  requires breaking the symmetries that protect them. Specifically, since these gapless points are stabilized by both sublattice (or inversion) symmetry and time-reversal symmetry, a gap can only emerge if at least one of these is broken.

A natural, yet naive, first approach to open a gap with such intent is to break sublattice symmetry. As previously discussed, the simplest way to do this is by assigning an apposite onsite energy  $\varepsilon$  to the  $A$  or  $B$  sites respectively, i.e  $\varepsilon_A = \varepsilon$  and  $\varepsilon_B = -\varepsilon$ . While this successfully gaps out the Dirac points, on quickly realizes that it leads to a rather uninteresting scenario. Taking the limit  $|\varepsilon| > t$ , the electronic states become strongly localized on one sublattice or the other, regardless of the sign of  $\varepsilon$ . Crucially, this configuration will not support any edge states. The reason why is because this mass term preserves time-reversal symmetry, and as long as time-reversal symmetry remains intact, it is fundamentally impossible to generate chiral edge modes.

Another, more ingenious way to gap out the Dirac cones in graphene, which is the essence of today's model, involves introducing a complex second-neighbor hopping term  $t'$ . The resulting Hamiltonian is known as Haldane's model and is given by

$$\begin{aligned} H_{\text{TB}}(\mathbf{R}) &= H_{\text{onsite}}^{(A)} + H_{\text{onsite}}^{(B)} + H_{\text{hopping}}^{(\text{NN})} + H_{\text{hopping}}^{(\text{NNN})} \\ &= \sum_i \epsilon_A a_{\mathbf{r}_i}^\dagger a_{\mathbf{r}_i} + \sum_i \epsilon_B b_{\mathbf{r}_i}^\dagger b_{\mathbf{r}_i} - t \sum_{\langle i,j \rangle} (a_{\mathbf{r}_i}^\dagger b_{\mathbf{r}_i+\delta_j} + b_{\mathbf{r}_j}^\dagger a_{\mathbf{r}_i-\delta_j}) - it' \sum_{\langle\langle i,j \rangle\rangle} (a_{\mathbf{r}_i}^\dagger a_{\mathbf{r}_i+\delta_j} - b_{\mathbf{r}_j}^\dagger b_{\mathbf{r}_i+\delta_j}) \end{aligned} \quad [55]$$

with  $\langle\langle i,j \rangle\rangle$  denoting the NNN sites. As illustrated in figure [11], the NNN hopping between  $A$  sites is taken as  $+it'$  while the NNN hopping  $B$  sites are taken in the opposite direction, being assigned  $-it'$ . A few key features of these second-neighbor hoppings are worth highlighting. First, see that all the (purely imaginary) hopping amplitudes possess the same chirality, i.e their orientation follows the direction of the reader's right hand's fingers when the thumb points out of the plane of the lattice. Second, these hoppings connect within the same sublattice,  $A$  to  $A$  and  $B$  to  $B$ .

Note that even a *real* second-neighbor hopping term would break particle-hole symmetry. This is acceptable because particle-hole symmetry is not an intrinsic property of real graphene, but rather a consequence of restricting hoppings to nearest neighbors. The crucial point is that breaking time-reversal symmetry requires the NNN hopping to be complex. Specifically, the hopping amplitudes acquire a direction-dependent phase, either being  $+it'$  when hopping clockwise or  $-it'$  when hopping counterclockwise, relative to the six-fold rotational axis at the center of the unit cell. This asymmetry between forward and backward hopping along these paths is the signature of time-reversal symmetry breaking.

When a gap opens at the Dirac points, the low-energy excitations are described by a massive Dirac equation. A crucial aspect of this mass term, represented by the  $\sigma_z$  Pauli matrix, is that it is chiral, meaning it carries a handedness or chirality. This chirality is related to the algebraic structure of the Pauli matrices  $\sigma_z = -i\sigma_x\sigma_y$  which encodes a handedness in the two-dimensional spinor space. **This needs context.** The behavior of the mass terms at the two Dirac points depends on which symmetry is broken. If only inversion symmetry is broken, the two Dirac points will still remain related by time-reversal symmetry, and since time-reversal reverses chirality, the masses at the two Dirac points will have opposite signs. This results in no net chirality as the contributions from the two valleys cancel out. Conversely, if only time-reversal symmetry is broken, the two Dirac points will still be connected by inversion symmetry, which preserves chirality in two dimensions. In this scenario, the masses at both Dirac points have the same sign, resulting in a non-zero net chirality, thus characterizing a nontrivial topological phase.

### 3. Gap closings are sources of Berry curvature

Before proceeding, let us briefly recall the concepts of Berry curvature and Chern number from section [??]. In that section, we studied the adiabatic time-evolution of a quantum state  $|\phi(\alpha)\rangle$  looping

around its parametric phase-space, returning to its initial configuration over a total time  $t = T$  along a path  $\mathcal{C}$ . Now, let  $\alpha$  be the crystal momentum  $\mathbf{k}$ , spanning over the Brillouin zone of the system. We saw that such a state accumulates over time a  $\exp\left(-i \int_0^T \varepsilon(\mathbf{k}(t)) dt\right)$  phase, but in addition, also a geometric phase  $\gamma_{\mathcal{C}} = \int_{\mathcal{C}} \mathbf{A}(\mathbf{k}) \cdot d\mathbf{k}$ , known as the Berry phase, with  $\mathbf{A}(\mathbf{k}) = \langle \phi(\mathbf{k}) | \nabla_{\mathbf{k}} | \phi(\mathbf{k}) \rangle$  the Berry connection. As the geometric nomenclature suggests, its value depends only on the path taken, not on how the said path was performed in time. The Berry curvature, defined as  $\Omega(\mathbf{k}) = \nabla_{\mathbf{k}} \times \mathbf{A}(\mathbf{k})$ , then followed as the local quantity that does not suffer from the ambiguities of the Berry connection gauge. Making use of Stokes theorem over the Brillouin zone folded in the shape of a torus we had concluded that

$$\iint_{BZ} \Omega(\mathbf{k}) \cdot d\mathbf{S} = \gamma(2\pi) - \gamma(0) = 2\pi W, \quad \text{with } W \in \mathbb{Z}$$

the so-called Chern number topological.

It is important to emphasize that the Berry phase is ill-defined for non-gapped systems. This means that the Chern number can only be computed for an isolated energy band that does not intersect any others. To deepen our intuition on this matter, it is useful to recall the analogy between Berry curvature and an electromagnetic field. Loosely speaking, a nonzero Chern number is analogous to the presence of a magnetic monopole, as it represents a net flux emerging from a closed surface. Moreover, just as one cannot define the electric flux through a surface if an electric charge sits exactly on it because the electric field becomes singular at the location of the charge, we similarly cannot define the Berry curvature at points where energy bands touch. In this sense, the Dirac points in our Haldane model bands act as the "sources" or "sinks" of Berry curvature in momentum space. Note, however, that this magnetic monopole analogy for the Berry curvature at the Dirac points is not general but rather a special feature of the Haldane model. In general, such an intuition cannot be applied because the specific distribution of the Berry curvature depends on the details of the Hamiltonian and thus varies significantly from model to model.

In figure [11](b) we present a schematic representation of the band structure and Berry curvature of the Haldane model, plotted as function of the ratio  $t'/\varepsilon$ . As a concrete example of the general principles discussed above, see that, for  $t'/\varepsilon > -1/3\sqrt{3}$ , Why  $-1/3\sqrt{3}$ ? Exercise to the reader. the former Dirac point at  $K$  acts as a source of (positive) Berry curvature. Conversely, for  $t'/\varepsilon < 1/3\sqrt{3}$ , the former Dirac point at  $K'$  acts as a sink of (negative) Berry curvature. We can see this by looking at the one-dimensional band structure of a ribbon of graphene. At the in-between regime  $t'/\varepsilon = 0$ , the contributions to the Berry curvature from the two Dirac points cancel out resulting in a total Chern number of zero. Most importantly, when the gap closes at either of the two Dirac points, chiral edge states appear! On the other hand, for  $|t'/\varepsilon| > 1/3\sqrt{3}$ , both Dirac points contribute Berry curvature of the same sign, resulting in a nontrivial topological phase with total Chern number  $W = \pm 1$ . Because the number of Dirac points in the Brillouin zone is an even number of two, and because  $K$  contributes positively to a Berry curvature of  $1/2$  and  $K'$  negatively, this ensures that the Chern number remains quantized an integer and changes by exactly one. Why  $1/2$ ? Exercise to the reader.

#### 4. Chiral edge states in graphene zigzag ribbons

As we just discussed, when the gap closes at either of the two Dirac points, chiral edge states emerge. To demonstrate that these states are of topological origin, let us consider the one-dimensional band structure of graphene ribbons with zigzag edges, as depicted in figure [11].

When a two-dimensional (2D) graphene sheet is cut into a ribbon, translational symmetry is preserved along the ribbon's longitudinal axis but broken in the transverse direction. Consequently, the system transitions from a 2D Brillouin zone (BZ), characterized by the Bloch momentum  $\phi = (\phi_1, \phi_2)$ , to a one-dimensional (1D) projected Brillouin zone with a single Bloch momentum component  $\phi$  along

the ribbon axis. The manner in which the valleys at  $K$  and  $K'$  are projected onto this 1D BZ depends on the ribbon's orientation, dictated by its edge termination. In the case of a zigzag configuration, the ribbon axis is aligned parallel to the  $K' - \Gamma - K$  direction in the 2D BZ. As a result, the two valleys are folded onto distinct points in the 1D BZ, yielding two separate and uncoupled valley features in the corresponding 1D band structure. By contrast, if the ribbon is cut in an armchair configuration, instead with its axis oriented perpendicular to the  $K' - \Gamma - K$  direction, the two valleys are folded onto the same point in the 1D Brillouin zone. This overlap induces hybridization between valley states in the 1D band structure, unless protected by additional symmetries that forbid such mixing.

Let us begin our analysis by examining the zigzag configuration within the nearest-neighbor hopping model, which, as previously discussed, preserves particle-hole symmetry. In this model, the zigzag edge introduces an imbalance in the number of sites belonging to each sublattice. Specifically, there is one extra site of a given sublattice for every three edge unit cells, due to the unit cell being effectively halved at the boundary. In contrast, the bulk, constrained by particle-hole symmetry, requires equal numbers of sites from both sublattices. Hence, for both of these conditions to hold consistently, any local excess of one sublattice at the edge must manifest as zero-energy modes between the two Dirac points (see the translucent, trivial band structure in figure [11]). Consequently, when a gap eventually opens, these edge states must remain connected to either the conduction or valence band at each of the two Dirac point projections. This results in four distinct configurations, all illustrated in figure [11]. This observation allows us to distinguish between two distinct scenarios, depending on whether spatial inversion symmetry or time-reversal symmetry is broken. If, upon gap opening, the edge states connect at the Dirac points the valence band to the valence band or the conduction band to the conduction band, then spatial inversion symmetry is broken, as the band structure is no longer symmetric about the Fermi level. This case is not of particular interest here. On the other hand, if time-reversal symmetry is broken, the edge mode instead connects the valence and conduction bands, forming a conducting channel across the gap. This is a fundamental consequence of the chiral anomaly associated with the quantum Hall effect. According to the bulk-edge correspondence, a non-zero net Chern number of the occupied bulk bands implies the existence of two chiral quantum anomalies at the edges: one associated with non-conservation of charge density, and the other with non-conservation of momentum density parallel to the edge.

#### *Flow of chiral edge states*

Let us further consider the case where one allows a magnetic flux  $\Phi$  is threaded through the bulk region of the graphene ribbon, as shown in figure [11]. When the flux is increased incrementally by one Dirac flux quantum  $\Phi_0 = \hbar/e$ , exactly one state is transferred, either from the conduction band to the valence band or vice versa, depending on the sign of the quantum Hall effect. Therefore, for such a state transfer to occur within this model, a chiral edge state must exist and propagate unidirectionally along the ribbon.

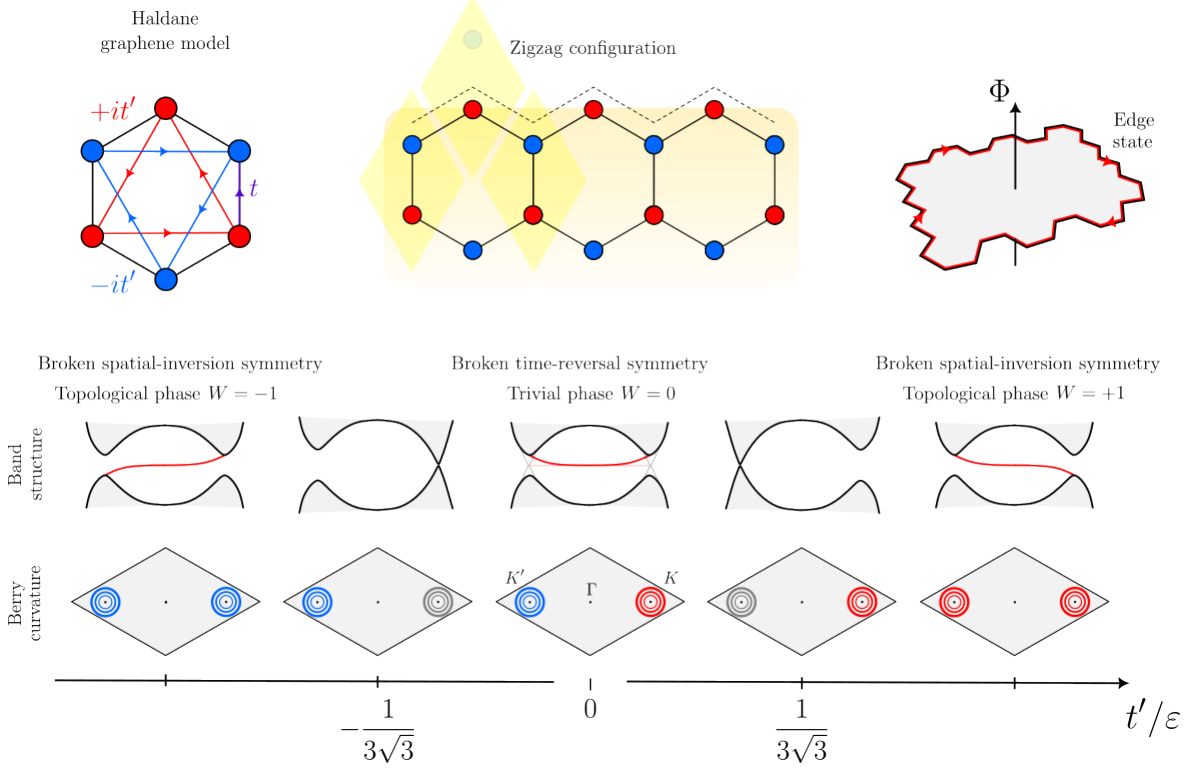


Figure 11. Haldane model tight-binding hoppings. Blue berry curvature indicates a positive value and red a negative one.

### C. Quantum spin Hall effect

Haldane's second video on the anomalous Hall effect makes a great transition.

#### 1. Kane-Mele graphene model

### D. Fractional quantum hall effect

# Part II

## Appendix

### IV. OVERVIEW OF GRAPHENE SYSTEMS

#### A. Standard monolayer graphene

Hexagonal boron nitride (hBN) is a 2D material composed of a simple layer of alternating boron and nitrogen atoms disposed in a planar honeycomb lattice, as shown in figure [13](a). The Bravais lattice

$$\mathbf{r}_i = n_{i1}\mathbf{a}_1 + n_{i2}\mathbf{a}_2, \quad n_{i1}, n_{i2} \in \mathbb{Z} \quad [56]$$

is generated by the real vectors basis

$$\mathbf{a}_1 = a_0 \begin{bmatrix} +\sin(30^\circ) \\ +\cos(30^\circ) \end{bmatrix} \text{ and } \mathbf{a}_2 = a_0 \begin{bmatrix} +\sin(30^\circ) \\ -\cos(30^\circ) \end{bmatrix}. \quad [57]$$

where  $\sin(30^\circ) = 1/2$  and  $\cos(30^\circ) = \sqrt{3}/2$ . In each diamond shaped Wigner-Seitz primitive cell (depicted in yellow), we have one boron atom and one nitride atom, which we designate as sub-lattices  $A$  (depicted in red) and  $B$  (depicted in blue) respectively. The atoms within the central primitive cell are located at

$$\mathbf{s}_A = \frac{a_0}{\sqrt{3}} \begin{bmatrix} 0 \\ -1/2 \end{bmatrix} \text{ and } \mathbf{s}_B = \frac{a_0}{\sqrt{3}} \begin{bmatrix} 0 \\ +1/2 \end{bmatrix}. \quad [58]$$

where the origin is defined at the midpoint between the atoms. For each site  $A$ , the position of the nearest-neighbors (NN) in the sites  $B$  are given by

$$\boldsymbol{\delta}_1 = \frac{a_0}{\sqrt{3}} \begin{bmatrix} 0 \\ 1 \end{bmatrix}, \quad \boldsymbol{\delta}_2 = \frac{a_0}{\sqrt{3}} \begin{bmatrix} +\sin(60^\circ) \\ -\cos(60^\circ) \end{bmatrix} \text{ and } \boldsymbol{\delta}_3 = \frac{a_0}{\sqrt{3}} \begin{bmatrix} -\sin(60^\circ) \\ -\cos(60^\circ) \end{bmatrix}. \quad [59]$$

where  $\sin(60^\circ) = \sqrt{3}/2$  and  $\cos(60^\circ) = 1/2$ . All these vectors are shown in figure [13](a) within the real space lattice. Furthermore, from the real lattice basis vectors, in order to fulfill  $\mathbf{a}_i \cdot \mathbf{b}_j = 2\pi\delta_{ij}$ , the reciprocal lattice basis vectors follow as

$$\mathbf{b}_1 = \frac{2\pi}{a_0} \begin{bmatrix} +\cos(30^\circ) \\ -\sin(30^\circ) \end{bmatrix} \text{ and } \mathbf{b}_2 = \frac{2\pi}{a_0} \begin{bmatrix} +\cos(30^\circ) \\ +\sin(30^\circ) \end{bmatrix}. \quad [60]$$

These are also shown in figure [13](b) together with the first zone of Brillouin, formed by the area enclosed by the intersection of their bisectrices. The high-symmetry points are  $\Gamma$ , the origin, the Dirac points  $K_\pm$  and  $M$  read as

$$\boldsymbol{\Gamma} = \begin{bmatrix} 0 \\ 0 \end{bmatrix}, \quad K_\pm = \pm \frac{4\pi}{3a_0} \begin{bmatrix} 1 \\ 0 \end{bmatrix} \text{ and } M = \frac{2\pi}{a_0} \begin{bmatrix} +\cos(30^\circ)/2 \\ +\sin(30^\circ)/2 \end{bmatrix} \quad [61]$$

where the  $K$  point is found such that  $(\mathbf{M} + K_{k_x} \hat{\mathbf{M}}_\perp)_{k_y} = 0$ , with  $\hat{\mathbf{M}}_\perp$  the unit vector in the perpendicular direction to  $\mathbf{M}$ . In far right side of figure [12], we make a note that the discretized grid it's

in the Bloch momentums basis  $\{\phi_1, \phi_2\}$ , i.e in the direction of the reciprocal lattice vectors, and not simply in the reciprocal space  $\{k_x, k_y\}$ . In the Bloch momentums basis the Dirac points would reads as  $K_{\pm} = 2\pi/3a_0 [\pm 1, \mp 1]$ .

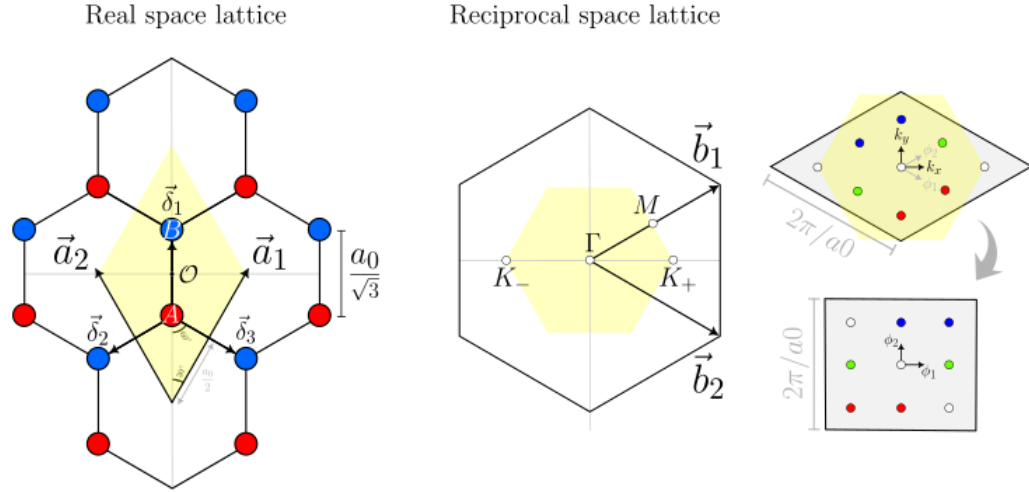


Figure 12.

Let us consider the nearest-neighbors (NN) tight-binding model, written in real space as

$$H_{\text{TB}}(\mathbf{R}) = H_{\text{onsite}}^{(A)} + H_{\text{onsite}}^{(B)} + H_{\text{hopping}}, \quad [62]$$

$$= \sum_i \epsilon_A a_{\mathbf{r}_i}^\dagger a_{\mathbf{r}_i} + \sum_i \epsilon_B b_{\mathbf{r}_i}^\dagger b_{\mathbf{r}_i} - t \sum_{\langle i,j \rangle} (a_{\mathbf{r}_i}^\dagger b_{\mathbf{r}_i+\delta_j} + b_{\mathbf{r}_j}^\dagger a_{\mathbf{r}_i-\delta_j}), \quad [63]$$

where the operators  $a_{\mathbf{r}_i}^\dagger (a_{\mathbf{r}_i})$  create (annihilate) an electron in the sub-lattice  $A$  in a given Bravais lattice site  $\mathbf{r}_i$ , the operators  $b_{\mathbf{r}_i}^\dagger (b_{\mathbf{r}_i})$  the same but for sub-lattice  $B$ ,  $\epsilon_A$  and  $\epsilon_B$  are the onsite energies of site  $A$  and  $B$  respectively, and  $t$  is the hopping strength between nearest-neighbouring sites  $A$  and  $B$  and back, denoted with  $\langle i,j \rangle$ .

Expressing the creation/annihilation operators as their Fourier counterparts,

$$a_{\mathbf{R}_i} = \frac{1}{\sqrt{V}} \sum_{\mathbf{k}} e^{i\mathbf{k}\cdot(\mathbf{R}_i+\mathbf{s}_A)} a_{\mathbf{k}} \quad \text{and} \quad b_{\mathbf{R}_i} = \frac{1}{\sqrt{V}} \sum_{\mathbf{k}} e^{i\mathbf{k}\cdot(\mathbf{R}_i+\mathbf{s}_B)} b_{\mathbf{k}}, \quad [64]$$

and using the identity  $\delta(\mathbf{k} - \mathbf{k}') = 1/N \sum_i e^{-i\mathbf{R}_i \cdot (\mathbf{k} - \mathbf{k}')}$ , we obtain the Hamiltonian in reciprocal space,

$$H_{\text{TB}}(\mathbf{R}) = \sum_{\mathbf{k}} \epsilon_A a_{\mathbf{k}}^\dagger a_{\mathbf{k}} + \sum_{\mathbf{k}} \epsilon_B b_{\mathbf{k}}^\dagger b_{\mathbf{k}} - t \sum_{\mathbf{k}} (\gamma_{\mathbf{k}} a_{\mathbf{k}}^\dagger b_{\mathbf{k}} + \gamma_{\mathbf{k}}^\dagger b_{\mathbf{k}}^\dagger a_{\mathbf{k}}), \quad [65]$$

where  $\gamma_{\mathbf{k}} = \sum_{\langle j \rangle} \exp(+i\mathbf{k} \cdot \delta_j)$  is complex number. If we now define a row vector  $c_{\mathbf{k}}^\dagger = [a_{\mathbf{k}}^\dagger \ b_{\mathbf{k}}^\dagger]$  we can rewrite the system's Hamiltonian as  $H_{\mathbf{R}}^{\text{TB}} = \sum_{\mathbf{k}} c_{\mathbf{k}}^\dagger H_{\mathbf{k}}^{\text{TB}} c_{\mathbf{k}}$  with

$$H_{\text{TB}}(\mathbf{k}) = \begin{bmatrix} \epsilon_A & -t\gamma_{\mathbf{k}} \\ -t\gamma_{\mathbf{k}}^\dagger & \epsilon_B \end{bmatrix}. \quad [66]$$

Within this simplified tight-binding model, the expression for the electronic two-band structure can easily be obtained analytically by diagonalizing the matrix in equation [66], yielding

$$E_{\text{TB}}^{\pm}(\mathbf{k}) = \pm \sqrt{\epsilon^2 + t^2 \left[ 3 + 2 \cos(a_0 k_x) + 4 \cos\left(\frac{a_0 \sqrt{3}}{2} k_y\right) \cos\left(\frac{a_0}{2} k_x\right) \right]}, \quad [67]$$

having defined the zero point energy at  $(\epsilon_A + \epsilon_B)/2$  and defined  $\epsilon \equiv (\epsilon_A - \epsilon_B)/2$  at the middle of the gap such that  $\epsilon_A = \epsilon$  and  $\epsilon_B = -\epsilon$ . The valence band corresponds to the  $E_{\text{TB}}^-(\mathbf{k})$  dispersion while the  $E_{\text{TB}}^+(\mathbf{k})$  corresponds to the conduction band, as shown in figure[13](c). The band structure is accompanied by the density of states  $\text{DoS}(E) = \sum_{\mathbf{k}} \delta(E - E(\mathbf{k}))$ .

Notice that, if  $\epsilon_A = \epsilon_B$ , as is the case for graphene, we obtain  $\epsilon = 0$  and the band dispersion closes in a linear fashion at the so called Dirac points. In hBN, the electronic band dispersion is also at its minimum near these points but has instead a parabolic shape. In either case, these points represent a fundamental symmetry of the system, called valley parity. To see why the dispersion is parabolic at these valley points, we Taylor series expand the exponential of  $\gamma_{\mathbf{k}}$  in equation [??] near  $\mathbf{k} \rightarrow \mathbf{K} + \mathbf{p}$  with  $\mathbf{p} \rightarrow 0$ . We obtain  $\exp(+i\mathbf{p} \cdot \boldsymbol{\delta}_j) \approx 1 + i\mathbf{p} \cdot \boldsymbol{\delta}_j$ . Now, since  $\sum_{\langle j \rangle} \exp(+i\mathbf{K} \cdot \boldsymbol{\delta}_j) = 0$  we are left with  $\gamma_{\mathbf{K} + \mathbf{p}} \simeq i\mathbf{p} \cdot \sum_{\langle j \rangle} \exp(+i\mathbf{K} \cdot \boldsymbol{\delta}_j) \boldsymbol{\delta}_j = -\sqrt{3}a_0/2(p_x - ip_y)$ . Invoking the Pauli matrices definitions, from equation [66] we can write the TB Hamiltonian  $H_{\text{TB}}^{\mathbf{k}}$  in this low-energy regime as

$$H_{\text{TB}}(\mathbf{K} + \mathbf{p}) = \epsilon \sigma_z + t \frac{\sqrt{3}a_0}{2} (\mathbf{p} \cdot \boldsymbol{\sigma}), \quad [68]$$

which clearly resembles the 2D Dirac Hamiltonian,  $H_{\text{Dirac}} = \sigma_z mc^2 + c(\mathbf{p} \cdot \boldsymbol{\sigma})$  with  $\epsilon$  taking the role of the rest mass energy  $mc^2$  and instead with a velocity  $v_F = t\sqrt{3}a_0/2$ , termed the *Fermi velocity*, as a replacement to the velocity of light  $c$ . Notice that, for the case of graphene, since  $\epsilon = 0$ , the electrons would behave as if they are massless. In this limit, the hBN low-energy dispersion can be written as the typical relativistic dispersion relation

$$E_{\text{TB}}(\mathbf{K} + \mathbf{p}) = \pm \sqrt{p^2 v_F^2 + m_{\text{eff}}^2 v_F^4}. \quad [69]$$

where  $m_{\text{eff}}$  is the effective mass of the electron at a given point near the valleys.

Refazer esta figura em Quantica para aprender a fazer densidade de estados. Falar das singularidades de van Hove.

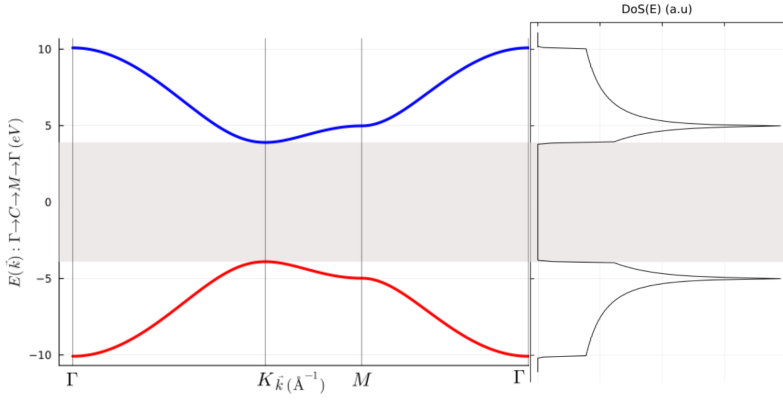


Figure 13. hBN electronic band structure from a nearest-neighbor tight-binding model accompanied by the density of the states. The dispersion goes along the symmetry path  $\mathbf{k} : \Gamma \rightarrow C \rightarrow M \rightarrow \Gamma$  and was calculated using  $\epsilon_g = 7.8\text{eV}$  for the energy gap,  $t = 3.1\text{eV}$  for the hopping parameter and  $a_0 = 1.42\sqrt{3}\text{\AA}$  for the honeycomb lattice length. **I could had here the contour band structure within the 1BZ Bloch phase space with the symmetry path.**

### B. Kekulé modulation

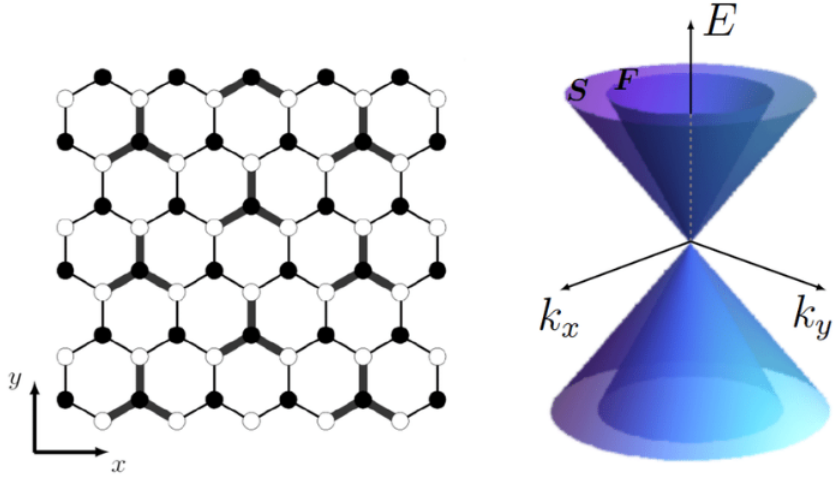


Figure 14. Caption

### C. Bilayer graphene

#### 1. Bernal bilayer graphene

Consider a bilayer graphene model depicted in figure [15].

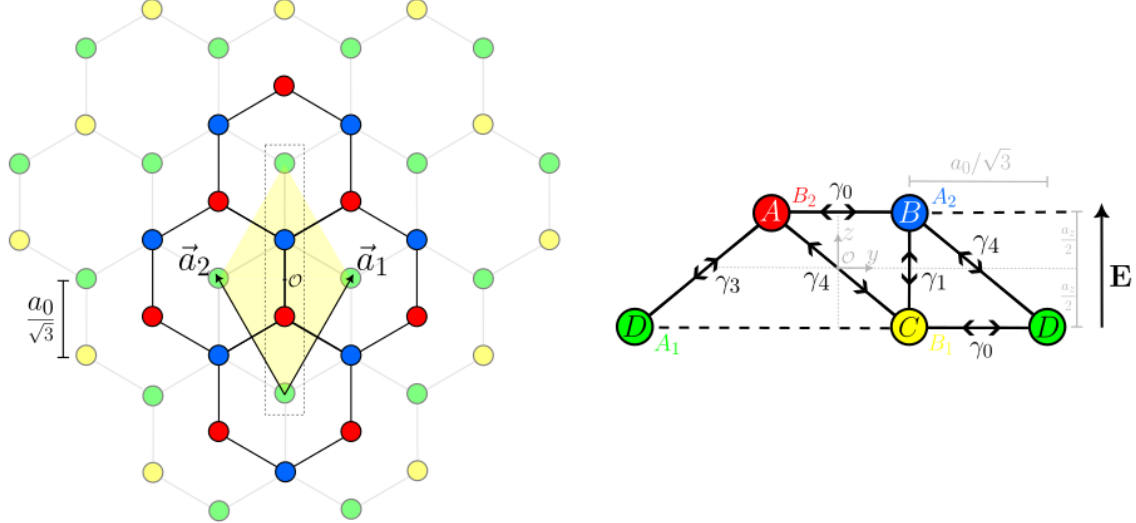


Figure 15. (a) Top view of the bilayer graphene (b) Side view of the dotted region in (a)

The tight-binding Hamiltonian of such a model reads

$$\begin{aligned}
H_{\text{BLG}} &= H_{\text{intralayer}} + H_{\text{interlayer}} = (H_{\text{top}} + H_{\text{bot}}) + (H_{\gamma_1} + H_{\gamma_3} + H_{\gamma_4}) \\
H_{\text{top}} &= \sum_i (\epsilon_A - \mu) c_i^\dagger a_i + \sum_i (\epsilon_B - \mu) b_i^\dagger b_i - \gamma_0 \sum_{\langle i,j \rangle} (a_i^\dagger b_j + h.c.) \\
H_{\text{bot}} &= \sum_i (\epsilon_C - \mu) c_i^\dagger c_i + \sum_i (\epsilon_D - \mu) d_i^\dagger d_i - \gamma_0 \sum_{\langle i,j \rangle} (c_i^\dagger d_j + h.c.) \\
H_{\gamma_1} &= +\gamma_1 \sum_{\langle i,j \rangle} (b_i^\dagger c_j + h.c.) \\
H_{\gamma_3} &= -\gamma_3 \sum_{\langle i,j \rangle} (a_i^\dagger d_j + h.c.) \\
H_{\gamma_4} &= +\gamma_4 \sum_{\langle i,j \rangle} (b_i^\dagger d_j + h.c.) + t_4 \sum_{\langle i,j \rangle} (a_i^\dagger C_j + h.c.)
\end{aligned}$$

Here, a site located at  $\mathbf{r}_i$  is indexed by the side index  $i$  and its next nearest neighbors located at  $\mathbf{r}_j$  are indexed with the site index  $j$ . Of course,  $\mathbf{r}_j$  depends on the kind of hopping in question: for  $\gamma_0$  it's  $\mathbf{r}_j = \mathbf{r}_i + \boldsymbol{\delta}_j$  with  $j = 1, 2, 3$ , for  $\gamma_1$  it's  $\mathbf{r}_j = \mathbf{r}_i \pm a_z \hat{\mathbf{z}}$ , and for  $\gamma_3$  and  $\gamma_4$  it's  $\mathbf{r}_j = \mathbf{r}_i + \boldsymbol{\delta}_j \pm a_z \hat{\mathbf{z}}$ . Moreover, let us consider an electric field  $\mathbf{E}$  uniform in the plane  $xOy$  and growing along the  $\hat{\mathbf{z}}$ , described by the tight-binding Hamiltonian

$$H_E = \sum_i E_i (f_{i\uparrow}^\dagger f_{i\uparrow} - f_{i\downarrow}^\dagger f_{i\downarrow})$$

where  $E_i = E \times z_i$  is the amplitude of the electric field at position  $\mathbf{r}_i$ , only really dependent on  $z_i$ , and  $f_i^\dagger = [f_{i\uparrow}^\dagger \ f_{i\downarrow}^\dagger]$  is a generic fermionic operator. Since in our bilayer model the bottom layer is situated at  $z = 0$  we redefine  $E(a_z) = E$ , such that

$$H_{\text{BLG}+} = E \sum_i \left\{ (a_{i\uparrow}^\dagger a_{i\uparrow} - a_{i\downarrow}^\dagger a_{i\downarrow}) + (b_{i\uparrow}^\dagger b_{i\uparrow} - b_{i\downarrow}^\dagger b_{i\downarrow}) \right\}$$

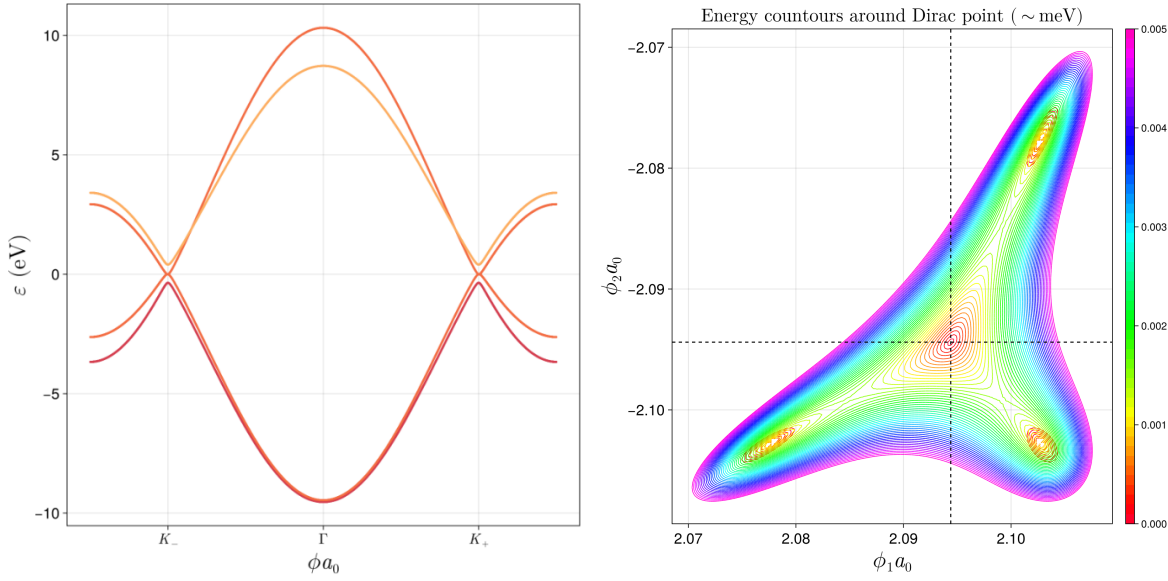


Figure 16. (a, b) Bandstructure along symmetry path  $\Gamma \rightarrow K_+ \rightarrow M$  and (c) trigonal warping of BLG around the Dirac point  $K_+$ .

## 2. Armchair and Zigzag configurations

### D. Twisted bilayer graphene

### E. Trilayer graphene

Make an image of the different stacking configurations ABC and ABA etc...

## Part III

# Bibliography

1. Fernandes's Lecture Notes: BCS theory of superconductivity for "BCS theory" section
  2. Tinkham's book at [Dover publisher link] for "Introduction to superconductivity theory" chapter
  3. Rashid's lecture notes at [personal website link] for "Introduction to superconductivity theory" chapter
  4. Akhmerov's online course at <https://topocondmat.org/> for "Introduction to topological superconductivity" chapter
  5. Asboth's short course at arXiv:1509.02295. for "Introduction to topological superconductivity" chapter
  6. Alejandro Pozo's thesis for "Kohn-Luttinger" section
  7. Tiago Antão's thesis at [uni repositoriun link] for "concepts of symmetry and topology" and the "SSH chain model" sections
  8. Kitaev's paper at Phys.-Usp. 44 131 for the "Kitaev model" and "Oreg-Lutchyn model" sections
  9. Lutchyn's at Phys. Rev. Lett. 105, 077001 for the "Kitaev model" and "Oreg-Lutchyn model" sections
  10. Oreg's at Phys. Rev. Lett. 105, 177002 for the "Kitaev model" and "Oreg-Lutchyn model" sections
  11. Cottam's book at MISSING for "Greens functions" appendix
  12. Kitaev's book at MISSING for "Greens functions" appendix
  13. Ming-Che Chang's notes at MISSING for "Greens functions" appendix
  14. Bruno Amorim's notes at MISSING for "Greens functions" appendix
- 

[1] One might get confused by the statement that "magnetic fields breaks time-reversal symmetry" since, if one considers the most basic Zeeman term  $H = -\boldsymbol{\mu} \cdot \mathbf{B}$ , both the magnetic moment  $\boldsymbol{\mu}$  and the magnetic field  $\mathbf{B}$  are odd under time reversal, meaning that the overall Hamiltonian would stay unchanged. This misunderstanding is in reality trivial to unravel since it only depends if one is considering whatever is producing  $\mathbf{B}$  as part of the system or not. If  $\mathbf{B}$  is internal to the system then the collective is symmetric under time reversal. If  $\mathbf{B}$  is instead considered an external perturbation to the system then time reversal will be broken (because one would simply not act with the time-reversal operator  $\mathcal{T}$  on  $\mathbf{B}$ ).